

1 Unequal anthropogenic enrichment of mercury in Earth's northern and
2 southern hemispheres.

3 Chuxian Li^{1,2}, Jeroen E. Sonke^{2§}, Gaël Le Roux¹, Natalia Piotrowska³, Nathalie Van der Putten⁴,
4 Stephen J. Roberts⁵, Tim Daley⁶, Emma Rice⁶, Roland Gehrels⁷, Maxime Enrico^{1,2,8}, Dmitri
5 Mauquoy⁹, Thomas P. Roland¹⁰, François De Vleeschouwer¹¹

6 *1. EcoLab, Université de Toulouse, CNRS, INPT, UPS, Toulouse, France.*

7 *2. Laboratoire Géosciences Environnement Toulouse, Université de Toulouse, CNRS, IRD, UPS, Toulouse, France.*

8 *3. Silesian University of Technology, Institute of Physics-CSE, Gliwice, Poland.*

9 *4. Faculty of Science, Vrije Universiteit Amsterdam, the Netherlands.*

10 *5. British Antarctic Survey, Cambridge, UK*

11 *6. School of Geography, Earth and Environmental Sciences, Plymouth University, Plymouth PL4 8AA, UK*

12 *7. Department of Environment & Geography, University of York, Heslington, York YO10 5NG, UK*

13 *8. Harvard John A. Paulson School of Engineering & Applied Sciences, Harvard University, Cambridge, MA, USA*

14 *9. Geography and Environment, School of Geosciences, University of Aberdeen, St Mary's Building, Aberdeen, AB24
15 3UF, UK*

16 *10. Geography, College of Life and Environmental Sciences, University of Exeter, UK*

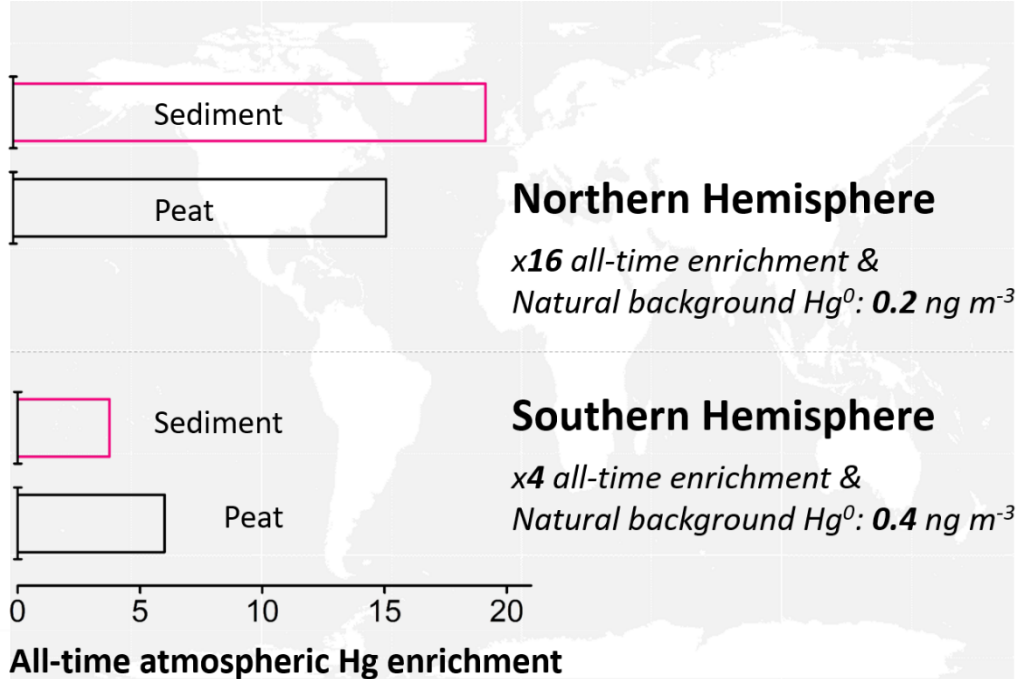
17 *11. Instituto Franco-Argentino para el Estudio delClima y sus Impactos (UMI 3351 IFAECI/CNRS-CONICET-UBA),
18 Universidad de Buenos Aires, Argentina*

19 [§] Corresponding author: jeroen.sonke@get.omp.eu

20

21

22 TOC Figure



23
 24 **Abstract:** Remote northern (NH) and southern hemisphere (SH) lake sediment and peat records of mercury
 25 (Hg) deposition show a $\times 3$ to $\times 5$ Hg enrichment since pre-industrial times (<1880AD), leading to the
 26 common perception that global atmospheric Hg enrichment is moderate and uniform. Anthropogenic Hg
 27 emission in the NH is, however, approximately four times higher than in the SH. Here we reconstruct
 28 atmospheric Hg deposition to four remote SH peatlands and review sediment and peat Hg records from
 29 both hemispheres. We observe a $\times 4$ enrichment in SH Hg deposition from pre-anthropogenic (<1450AD)
 30 to late 20th century periods, which is lower than the large $\times 16$ all-time enrichment in NH Hg deposition.
 31 We attribute this difference to lower anthropogenic Hg emissions in the SH, and higher natural
 32 atmospheric SH Hg concentrations, supported by $\times 2$ higher natural background Hg accumulation in SH
 33 peat records. We suggest that the higher SH natural Hg concentrations reflect the SH land-ocean
 34 distribution, with higher marine SH Hg emissions driven by transport of NH Hg to the SH by the Ocean
 35 conveyor belt. Our findings suggest that Hg background levels and anthropogenic enrichment in both
 36 hemispheres are different and must be taken into account in international Hg assessments and
 37 environmental policy.

38

39 **Introduction:**

40 Mercury (Hg) is a toxic trace metal that affects wildlife and human health ¹⁻⁴. Hg is discharged into the
41 environment by natural processes, such as volcanism, chemical and physical weathering, and by human
42 activities, including mining, coal burning and intentional use ⁵⁻⁷. Elemental Hg⁰, the dominant form of
43 emissions, has a long atmospheric residence time of 6 to 12 months, which allows for its intra-hemispheric
44 dispersion before being deposited to the Earth's surface, including remote environments ⁸. Assessments
45 of the extent of global Hg pollution have relied upon natural archives of Hg accumulation (e.g. sediment
46 ^{9,10}, peat ¹¹, ice cores ¹²), and on estimates of natural and anthropogenic Hg emissions ⁷.

47 Since early work on lake sediment cores in the 1970s ¹³, hundreds of remote ²¹⁰Pb dated sediment
48 cores have documented an approximate three- to five-fold increase in Hg accumulation rates (HgAR) from
49 pre-industrial (1760-1880 AD) times to the late 20th century ^{9,10,14-17}. A comprehensive review in 2007
50 concluded that sediment records were more reliable than peat records in recording atmospheric HgAR ¹⁵.
51 Inferred, higher Hg accumulation in peat records was thought to be related to ²¹⁰Pb mobility, and peat
52 mass loss during remineralization. A recent review study ¹⁶ indicated that earlier peat vs sediment
53 comparisons ¹⁵ used different reference periods to calculate Hg enrichment. Using coherent reference
54 periods, dozens of peat archives and a small number glacier ice cores of atmospheric deposition also
55 document 3 to 5-fold enrichment factors, similar to sediment records, since pre-industrial times (EF_{preind})
56 ^{14,16}. Both sediment and peat records have strengths and weaknesses, with ²¹⁰Pb and Hg mobility during
57 sediment diagenesis and peat decomposition being potential factors of bias ¹⁸⁻²⁰. Yet, both archives at
58 remote locations record broadly similar Hg accumulation profiles across the past millennium, despite
59 differences in archive functioning, and therefore warrant further comparison across Earth's two
60 hemispheres. Regarding archive functioning, lake sediments integrate Hg deposition to a larger watershed,
61 Hg storage in soils, followed by Hg run-off and in-lake cycling leading to a longer Hg residence-time before
62 deposition to sediments. Peatlands integrate Hg deposition directly from the atmosphere ^{16,21,22}, leading
63 to a more direct response of peat archives to atmospheric Hg⁰ concentrations. This can generally be
64 recognized by the 2-fold drop in HgAR from the 1970s to the 1990s in peat ¹⁶, which is absent in sediment
65 records, and which mirrors the well-documented decrease in Hg emissions and observed atmospheric Hg⁰
66 concentrations ^{7,23,24}. A comparison of Hg stable isotope composition of peat and lake sediments indicates
67 that in both media, 75% of Hg derives from uptake of atmospheric Hg⁰ ²¹, which further justifies comparing
68 both archives.

69 Longer radiocarbon-dated NH sediment and peat cores probe changes in the natural background Hg
70 accumulation during pre-colonial times (pre-1450AD), before large-scale mining practices, and indicate a

71 more dramatic difference in Hg deposition. Millennial sediment and peat records show that HgAR already
72 increased five-fold during the earlier transition from pre-large-scale mining to pre-colonial times around
73 approximately 1450 AD¹⁶. All-time anthropogenic Hg enrichment factors ($EF_{alltime}$, the ratio of 20th century
74 to pre-1450AD HgAR), determined in sediment and peat records therefore ranges from 16 to 26¹⁶. The
75 cause for the increase in NH Hg enrichment around 1450AD is debated. Some Hg inventory and modeling
76 studies have argued for enhanced Hg emissions from Spanish colonial silver and gold mining²⁵⁻²⁷. Other
77 studies argue that Hg associated with mining has been immobilized in mining waste, rather than volatilized
78^{1,28,29}. A study on Hg stable isotopes in peat has recently shown evidence how enhanced deforestation
79 during the Middle Ages may have impacted regional atmospheric Hg dynamics in Europe with lower
80 vegetation uptake of Hg, and wood burning emissions leading to enhanced atmospheric Hg concentrations
81 and deposition²³. What nearly all the above cited studies have in common, is that they are situated in the
82 northern hemisphere (NH) where the majority of historical anthropogenic Hg emissions have taken place
83 and have been abundantly investigated. Relative to the NH, anthropogenic Hg emissions in the SH have
84 continuously been four times lower³⁰. Reviews of anthropogenic Hg enrichment in the environment
85 generally provide a global picture without discerning the hemispheres^{18,31-33}. Lake sediment records of Hg
86 accumulation have been studied in the SH and will be reviewed here. Three southern hemisphere (SH)
87 peat records have been studied for HgAR^{34,35}, but are all incomplete (see Methods, and Extended Data 2)
88 and preclude a rigorous assessment of SH atmospheric Hg enrichment based on both sediment and peat
89 archives.

90 The aim of this study was therefore to investigate differences in anthropogenic Hg enrichment, if any,
91 in Earth's SH and NH. We hypothesize that, in regard of the lower historical SH anthropogenic Hg emissions,
92 enrichment will also be lower. We extend the limited number of peat archives studied in the SH, by
93 investigating Hg accumulation rates in four new radiocarbon and ²¹⁰Pb and ¹⁴C bomb-pulse dated SH peat
94 records. We then review all the existing SH sediment and peat HgAR (Extended Data 2), compare Hg
95 enrichments factors to the NH, and discuss findings in the context of revised volcanic Hg emissions,
96 published historical anthropogenic Hg emissions, and Hg cycling in both hemispheres. We do not include
97 glacier ice cores in our review due to the limited number of studies available, and we do not consider
98 marine sediment records. Four reference time periods, operationally defined for NH natural archives
99 elsewhere^{16,17}, will be used throughout: natural background (pre-1450AD), pre-industrial period (1450-
100 1880 AD), 20th century extended HgAR maximum (20Cmax, approximately from 1940-1990; see also
101 Methods), and the recent post-1990 modern period.

102 **Methods**

103 **The study sites.** We investigate four new cores from remote ombrotrophic peat bogs in the SH mid-
104 latitudes: Amsterdam Island (AMS, S-Indian Ocean), Falkland Islands (SCB, San Carlos bog, Islas Malvinas,
105 S-Atlantic Ocean), Andorra and Harberton (AND, HAR, Tierra del Fuego, Argentina) (SI Appendix Table S1;
106 Figure S1; Text S1; Extended Data 1). These four sites are situated in the Southern Westerly wind belt, far
107 away from anthropogenic Hg sources, which makes them ideal recorders of SH remote atmospheric Hg
108 deposition trends. Details about the field campaigns and sampling sites are given in SI Appendix Table S1
109 and Text S1. After collection, all the cores were photographed, described and packed in plastic film and
110 PVC tubes and shipped to EcoLab, Toulouse, France. There, the cores were cut and processed following
111 published trace metal clean protocols, freeze-dried and stored dry until analysis^{36,37}.

112 **Chronology.** Age model output of the AMS peat core is adopted from³⁸. In brief, a total of 20 samples
113 were picked for plant macrofossils and subsequently radiocarbon-dated at the LMC14 Artemis Laboratory
114 (Saclay, France, SacA code) or GADAM center (Gliwice, Poland, GdA code). Recent age control in the AMS
115 peat core is based upon 4 post-bomb radiocarbon dates³⁹ together with ²¹⁰Pb dating using the constant
116 rate of supply model, and ¹³⁷Cs, ²⁴¹Am⁴⁰. A total of 9 samples of plant macrofossils/charcoal from SCB 10
117 and 13 samples of *Sphagnum* macrofossils from AND and HAR respectively, were radiocarbon dated. These
118 radiocarbon samples were pre-treated and graphitized at the GADAM center (Gliwice, Poland, GdA code)
119 ⁴¹. Subsequently, their ¹⁴C concentration in graphite was measured at the DirectAMS Laboratory (Bothell,
120 WA, USA; ⁴²). The NIST Oxalic Acid II standard was used for normalization, and black coal used as a blank.
121 A total of 22 samples from the top 62 cm of the SCB peat core were selected for ²¹⁰Pb measurement by
122 alpha counting to constrain the recent age (see Extended Data 1). The recent age control of the AND and
123 HAR peat cores derive from 5 and 10 post-bomb radiocarbon dates, respectively^{39,43}.

124 Details of radiocarbon dates are summarized in SI Appendix Table S2. Age-depth models were
125 generated from a combination of radiocarbon dating, post-bomb and ²¹⁰Pb dating with the Bacon package
126 within R software⁴⁴, using the SHCal13 calibration curve for positive ¹⁴C ages⁴⁵, while the post-bomb
127 radiocarbon dates were calibrated with SH zone 1-2 curve⁴⁶. The prior settings and model outputs are
128 presented in SI Appendix Figure S2. The modelled median age was used for calculating and plotting HgAR
129 against time (Figure 1). The average age uncertainties (1-sigma) derived from the age-depth models range
130 from 1-5 years for the topmost part of the cores, up to ca. 100 years around 1000 AD. The investigated
131 peat profiles of AMS, SCB, AND, and HAR cover periods of 6600, 2000, 200 and 800 years, respectively.
132 Corresponding mean peat accumulation rates are 0.76, 0.85, 3.6 and 0.91 mm yr⁻¹ respectively.

133 **Peat Hg accumulation rates (HgAR).** HgAR is calculated as the product of Hg concentration (ng g^{-1}), peat
134 density (g cm^{-3}) and peat mass accumulation rate ($\text{g m}^{-2} \text{yr}^{-1}$). Peat density was determined for each 1 cm
135 slice by measuring its volume using a Vernier caliper and dry peat mass after freeze-drying. Peat samples
136 were analyzed for total Hg (THg) concentration on a combustion cold vapor atomic absorption
137 spectrometer (CV-AAS, Milestone DMA-80) at the University of Toulouse, France. The IPE 176 CRM (Reed
138 / *Phragmites communis*), NIST 1632d (Coal), and BCR 482 (Lichen) were analyzed with mean recoveries
139 ranging from 93-100% (SI Appendix Table S3). Replicate/triplicate analyses of THg in peat samples were
140 found to vary by less than 6% (1σ). Profiles of peat Hg concentration in AMS, SCB, AND, and HAR are shown
141 in SI Appendix Figure S5. Peat mass accumulation rate was determined from the age models and dry peat
142 mass. All raw data is summarized in Extended Data 1.

143 **Literature review, reference time periods and statistics.** We expand on a previous literature review of
144 sediment and peat Hg archives³¹. We examined the remote HgAR records from SH lake sediments and
145 peat records in Southern South America, lake sediments in New Zealand, lake sediments in East Africa,
146 and lake sediments in Antarctica (see Extended data 2 for details). We did not retain: a lake sediment core
147 6 km downstream from the Potosi mine (Bolivia) with pronounced local mining influences on HgAR⁴⁸; a
148 lake sediment core in the Patagonian volcanic zone with multiple tephra layers associated with high HgAR
149⁴⁹. Two remote Bolivian cores and one Peruvian core also showed evidence for the release of Hg due to
150 regional Spanish colonial mining activities^{35,50}, but were retained in Extended Data 2. NH remote sediment
151 and peat records were updated from¹⁶. Extended Data 2 indicates which records were only partially used,
152 often due to lack of recent ²¹⁰Pb or ¹⁴C bomb pulse dates. This applies in particular to three SH peat records,
153 where one lacks a recent ²¹⁰Pb chronology and therefore 20Cmax and pre-industrial HgAR³⁵, one lacks pre-
154 1988 layers⁴⁷, and one is nearly complete³⁴, except for the 1826-1935 period, which we extrapolate (see
155 Extended Data 2).

156 We use four reference time periods, based on previous studies and which were originally
157 operationally derived for NH natural archives¹⁶: natural background (pre-1450AD), pre-industrial period
158 (1450-1880AD), 20th century extended HgAR maximum (20Cmax, approx. 1940-1990), and the recent,
159 modern period (post-1990AD). The operational cut-off years, e.g. 1450, 1880, 1990, are mean values based
160 on the remote NH sediment (n=49) and peat cores (n=19) reviewed here. In other words, each archive and
161 each regional context shows variation in the exact timing of gradual or abrupt increases (~1450, ~1880) or
162 decreases (~1990) in HgAR (Extended Data 2). Several long SH sediment records probe the effect of climate
163 change on variations in HgAR during the Holocene and since the last glacial maximum. Depending on

164 watershed type and location these studies document substantial natural variability in HgAR that is beyond
 165 the scope of this study, but no less important. Therefore, in order to assess to the best of our ability the
 166 impact of humans on recent, millennial atmospheric Hg enrichment, we integrated natural background
 167 HgAR between on average -1700BC to 1450AD, but on occasion as far back as 10,000BC (Extended Data
 168 2).

169 Statistical descriptions are parametric (mean, standard deviation (SD)) for normally distributed
 170 HgAR and enrichment factors (EF), and non-parametric (median, Q25% and Q75% quartiles, interquartile
 171 range (IQR)) for non-normally distributed HgAR and EF. Outlier tests were performed only on EFs, and
 172 observations were excluded (in *italics* in Extended Data 2) when they exceeded 2*SD around the mean, or
 173 1.5*IQR around Q25% and Q75%. All data generated or analyzed during this study are included in the SI
 174 Appendix.

175 **Results & Discussion**

176 HgAR profiles in the four SH peat records show maximum values during the 20th century (Figure 1). Natural
 177 background (pre-1450 AD) HgAR in the HAR, SCB and AMS cores show a mean of $4.9 \pm 3.5 \mu\text{g m}^{-2} \text{yr}^{-1}$ (mean,
 178 1σ , n=33 in 3 cores, Figure 1). Pre-industrial HgAR in the four cores averages $5.9 \pm 2.5 \mu\text{g m}^{-2} \text{yr}^{-1}$, 20Cmax
 179 HgAR is $20 \pm 7.9 \mu\text{g m}^{-2} \text{yr}^{-1}$, and modern HgAR is $9.7 \pm 2.9 \mu\text{g m}^{-2} \text{yr}^{-1}$ (means, 1σ , n=4, Figure 1). AND and
 180 HAR have more pronounced 20Cmax peaks than SCB and AMS, which is due to a combination of peaks in
 181 Hg concentration (Figure S5) and enhanced peat mass accumulation rate occurring simultaneously
 182 (Extended Data 1). Whereas absolute HgAR for the different time periods vary between cores, the relative
 183 HgAR changes between cores are similar and can be expressed by enrichment factors, EF. The four SH
 184 cores show evidence for 3.1-fold (mean, $1\sigma=1.6$) enhanced net Hg deposition during the 20Cmax,
 185 compared to the pre-industrial period (EF_{preind} , Table 1), which at first sight appears similar to NH natural
 186 archives. SH historical HgARs have thus far been studied in 20 lake sediment and 3 peat cores (see Methods
 187 and Extended Data 2 for full list). Figure 2 summarizes HgAR and EF in all published SH sediment and peat
 188 records, as well as updated NH data for the reference periods of interest (Extended Data 2). The temporal
 189 evolution of HgAR in peat and sediment cores is similar between the NH and SH in a broad sense (Figure
 190 2a, b). HgAR increases stepwise from natural background to pre-industrial and then to 20Cmax periods in
 191 both sediment and peat archives. Similar to NH peat records¹⁶, modern-day (post-1990) HgAR in SH peat
 192 decreases by a factor of 2 from 20Cmax values (SI Appendix Figure S4), in line with declining global
 193 anthropogenic Hg emissions and deposition from the 1970s to 2000s (Figure S6^{23,24}). Sediment records in

194 both the NH and SH do not record this decrease (Figure S4), presumably due to the longer residence of Hg
195 in lake catchment soils, leading to a slower recovery of Hg concentrations in soil run-off into lakes (15).

196 The historical evolution of trends in hemispheric HgARs are shown in EF_{preind} and $EF_{alltime}$ diagrams
197 (Figure 2c, 2d). Pre-industrial to 20Cmax enrichment in HgAR (EF_{preind}) is higher in peat compared to
198 sediment in both NH and SH (Kruskal-Wallis test, NH, $P=0.01$; SH, $P=0.10$). EF_{preind} is higher in the NH than
199 in the SH for sediment (3.1 vs 1.8), but not peat (4.6 vs 3.1; Kruskal-Wallis test, peat, $P=0.15$; sediment
200 $P=0.001$; Figure 2c, 2d; Figure 3a). We find in particular that in long, millennial NH records, HgAR increased
201 3.9-fold in peat and 3.7-fold in sediments across the natural background to pre-industrial periods ($EF_{p/b}$,
202 Figure 2c, d, Table 2). On the contrary, $EF_{p/b}$ in SH millennial records show negligible, mean 1.2-fold
203 enrichment in peat, to a small, median 1.4-fold enrichment in sediments across the natural background
204 (<1450AD) to pre-industrial periods. Consequently, all-time NH enrichment factors, $EF_{alltime}$, reach 16 in
205 peat and 13 in sediments and are larger than the 6.0-fold and 3.8-fold Hg all-time enrichment in SH peat
206 and sediments (Table 2; Figure 3B; Kruskal-Wallis test, $P = 0.02$ for peat, $P = 0.09$ for sediment). Historical
207 Hg emission inventory and associated box modeling studies have suggested that the 4-fold increase in NH
208 HgAR across around 1450AD is related to Spanish colonial Hg and silver mining^{7,25}. This interpretation has
209 been refuted by studies arguing that the associated emissions are overestimated^{1,28,51} SH archives show
210 little evidence of Spanish colonial mining impacts in South-America on large scale SH atmospheric Hg
211 deposition (Figure 2). Similarly, neither NH peat, nor sediment records show evidence of a pronounced
212 late 19th century peak in HgAR, in contrast to large estimated N-American gold-rush Hg emissions⁷. We
213 therefore suggest the 4-fold NH increase in HgAR around 1450AD is more likely related to demography
214 driven changes in land-use (e.g. deforestation, wood, peat combustion, urbanization etc. Enrico et al.,
215 2016), than to direct Spanish colonial mining emissions of Hg to the global pool. In summary, our findings
216 based on combined sediment and peat archive HgAR observations, suggest that all-time atmospheric Hg
217 enrichment during the 20Cmax period (1940-1990) reached 11-fold globally ($EF_{alltime} = 4-24$, 25%-75%
218 quartiles, $n=39$), 16-fold in the NH ($EF_{alltime} = 10-30$, 25%-75% quartiles, $n=26$), and 4-fold in the SH ($EF_{alltime}$
219 $= 2-6$, 25%-75% quartiles, $n=13$). Atmospheric Hg concentrations decreased from the 1970's to the 2000's
220 by a factor of about 2, a trend that is recorded in the peat archive HgAR (Figure S4, S6). Natural background
221 to modern period (1990-2010) Hg enrichment, $EF_{mod/bck}$, based on peat archives, is currently 10-fold
222 globally (± 7.7 , 1σ , $n=18$), 12 in the NH (± 7.5 , 1σ , $n=14$) and 3 in the SH (± 2.5 , 1σ , $n=4$).

223 In the following sections we will further discuss this sizeable difference in hemispheric $EF_{alltime}$ in terms
224 of NH and SH Hg emissions, and in terms of natural background HgAR. The all-time NH and SH enrichment

225 factors based on Hg deposition to natural archives can be directly compared to independent estimates of
226 NH and SH emission factors, i.e. EF_{emission} , the ratio of primary, i.e. first time, total Hg emission flux to
227 natural Hg emission flux ($EF_{\text{emission}} = F_{\text{anthro}} + F_{\text{natural}} / F_{\text{natural}}$; Table 3). In doing so, we make the assumption
228 that re-emission of previously deposited natural and anthropogenic Hg is proportional to primary
229 emissions. By separating NH and SH emission factors we also assume limited hemispheric exchange of
230 atmospheric Hg, supported by the short global lifetime of Hg of 5 months in state of the art atmospheric
231 Hg models⁸. This assumption may need to be revisited in the future as the debate on atmospheric Hg
232 lifetime continues due to new discoveries in Hg redox dynamics⁵². Global anthropogenic Hg emissions to
233 the atmosphere have been estimated at $2.4 \pm 0.5 \text{ Gg yr}^{-1}$ during the 20Cmax period (1940-1990)⁷. Natural
234 Hg emissions are the sum of volcanic degassing and crustal degassing from naturally enriched soils. Passive,
235 non-eruptive, volcanic degassing is an important direct natural source of Hg to the atmosphere, with a
236 previously estimated total flux of $76 \pm 30 \text{ Mg yr}^{-1}$ (1σ) based on observed Hg/SO₂ ratios of $7.8 \pm 1.5 \times 10^{-6}$
237 and a global passive degassing SO₂ flux of 9.7 Tg yr^{-1} ^{53,54}. Recent advances in remote sensing of SO₂ from
238 2005-2015 indicate a higher SO₂ flux of $23.0 \pm 2.3 \text{ Tg yr}^{-1}$ (1σ)⁵⁵, which we use here to revise the global
239 passive volcanic degassing Hg flux to $179 \pm 39 \text{ Mg yr}^{-1}$ (1σ). Eruptive volcanic SO₂ emissions are indicated
240 to be one order of magnitude smaller than passive degassing at $2.6 \pm 2.6 \text{ Tg yr}^{-1}$ ⁵⁵. Assuming similar Hg/SO₂
241 ratios, we estimate eruptive volcanic Hg emissions at $20 \pm 20 \text{ Mg yr}^{-1}$, and total volcanic Hg emissions as
242 the sum of eruptive and passive emissions at $200 \pm 60 \text{ Mg yr}^{-1}$ (1σ). Global emissions from naturally
243 enriched soils can be estimated from reviews of flux chamber and soil Hg studies^{56,57} and equal 135 ± 40
244 Mg yr^{-1} (1σ , Table 3). These bottom-up estimates indicate that global anthropogenic 20Cmax Hg emissions
245 of 2.4 Gg yr^{-1} have been 7.3 times larger than global natural Hg emissions of 0.34 Gg yr^{-1} , and result in a
246 global EF_{emission} of 8.2. Volcanic SO₂ emissions are similar for the NH and SH (11.8 vs. 11.2 Tg yr^{-1})⁵⁵, leading
247 to NH and SH Hg emission budgets of 0.1 Gg yr^{-1} each. We scale naturally enriched soil emissions with
248 continental surface area, to estimate 91 and 44 Mg yr^{-1} in NH and SH. The 20Cmax 2.4 Gg yr^{-1} global
249 anthropogenic Hg emissions to the atmosphere were released for 80% to the NH and 20% to the SH⁷. We
250 therefore estimate hemispheric EF_{emission} , for the NH at 11.2 ± 4.6 and for the SH at 4.4 ± 1.5 (1σ). The SH
251 EF_{emission} of 4.4 is in good agreement with the natural archive-based SH EF_{alltime} of 4. The NH EF_{emission} of 11
252 however, underestimates the NH EF_{alltime} of 16 by 43%, suggesting that either the $2.0 \pm 0.5 \text{ Gg yr}^{-1}$ NH
253 anthropogenic Hg emissions to air⁷ are underestimated, or that the NH natural primary emissions of $91 \pm$
254 27 Mg yr^{-1} are overestimated. There is a final caveat in this analysis that deserves a mention: We assume
255 that the ill-constrained, but potentially important, submarine volcanic Hg flux⁵⁸ is locally or regionally

256 deposited to marine sediments before any of it can be emitted to the atmosphere. This assumption is
257 based on evidence for Hg scavenging in submarine hydrothermal plumes^{59,60}.

258 The most recent, 2018 UNEP global Hg assessment, which provides the state of the science basis for
259 the implementation of the UNEP Minamata Convention on Mercury, states that “Human activities have
260 increased total atmospheric Hg concentrations by about 450% (i.e. a factor 4.5) above natural levels.”^[7].
261 Our findings therefore suggest that modern (1990-2010) atmospheric Hg enrichment is larger, 10-fold
262 globally. Contrary to presumed uniform global Hg enrichment, we also find consistently lower
263 anthropogenic Hg enrichment in emissions and in deposition in the SH compared to the NH.

264 The important difference in NH and SH $EF_{alltime}$ is not only related to hemispheric differences in
265 primary Hg emissions, but also to differences in natural background atmospheric Hg concentrations and
266 HgAR. A notable outcome of the new SH peat records is that the natural SH background HgAR of $4.3 \mu\text{g m}^{-2}$
267 yr^{-1} in the SH mid-latitudes (30-60°S) is $\times 2.5$ higher than the NH background HgAR of $1.7 \mu\text{g m}^{-2} \text{yr}^{-1}$ in the
268 NH mid-latitudes (Kruskal-Wallis test, $P=0.02$, Figures 2a, 3c, S3). Recent Hg stable isotope work on Hg
269 deposition to vegetation and soils suggests that 75% derives from direct uptake of atmospheric Hg^0 , and
270 less from Hg(II) wet deposition⁶¹⁻⁶⁴. We therefore suggest that the marked NH/SH mid-latitude difference
271 in HgAR is driven by $\times 2.5$ higher natural atmospheric Hg concentrations in the SH, rather than climate
272 factors. Climate factors, such as temperature and length of growth season only become visible in NH high
273 latitude ($>60^\circ\text{N}$), where HgAR becomes limited by peat bog primary productivity, via the vegetation Hg^0
274 pump (18). The observation that the SH natural background HgAR is $\times 2.5$ higher than the NH background
275 is likely an additional reason why the NH $EF_{alltime}$ of 16 is so much larger than the SH $EF_{alltime}$ of 4. Inter-
276 hemispheric trends in atmospheric Hg have been previously investigated^{65,66}. Observed mean atmospheric
277 Hg^0 concentrations across monitoring networks for the modern, 1990-2010 period were 1.8 ng m^{-3} in the
278 NH and 1.2 ng m^{-3} in the SH^{67,68}. Modern-day SH Hg^0 concentrations are therefore higher than what would
279 be expected based on estimates of modern NH and SH primary Hg emissions of 1.6 and 0.7 Gg yr^{-1} (Table
280 3). A key difference between the NH and SH is the land-ocean distribution, with the SH being only 19%
281 land covered and the NH 39%. The land-ocean distribution plays an important role in atmospheric
282 boundary layer Hg dynamics. A study on atmospheric Hg^0 seasonality, which is more pronounced in the
283 NH and quasi-absent in the SH, suggested that the vegetation Hg pump, i.e. the foliar uptake of Hg^0 and
284 sequestration in soils, is an important driver of NH atmospheric Hg^0 seasonality²². The SH has a smaller
285 terrestrial vegetation and soil pool, and we speculate that the SH has relatively higher atmospheric Hg^0
286 due to a weaker vegetation Hg pump. In addition coupled ocean-atmosphere Hg chemistry and transport
287 models find stronger marine Hg^0 evasion in the SH than in the NH, mainly due to upwelling of Hg rich deep

288 waters in the Southern Ocean^{17,69}. The model studies suggest that SH atmospheric Hg⁰ is largely controlled
289 by these SH marine Hg⁰ emissions^{8,17}. These findings were recently confirmed by long-term observations
290 on Hg⁰ seasonality at the Cape Point, South-Africa monitoring station⁷⁰. The 2-fold higher SH natural
291 background HgAR in peat therefore echoes the higher than expected modern SH atmospheric Hg⁰
292 concentrations, and both can potentially be explained by the hemispheric land-ocean distribution. We
293 suggest here that the Ocean conveyor belt plays an important role in shuttling NH marine Hg to the SH in
294 order to sustain the marine evasion driven, elevated natural atmospheric Hg concentrations in the SH.
295 Such a mechanism is supported by the long estimated deep Ocean Hg lifetime, in excess of 1000 yr¹⁷.

296 We use peat $EF_{\text{modern/back}}$ for both hemispheres (Table 2) to estimate what natural atmospheric Hg⁰
297 concentrations may have been during pre-1450AD times. Dividing modern-day mean NH and SH
298 atmospheric Hg⁰ concentrations of 1.8 and 1.2 ng m⁻³ by $EF_{\text{modern/back}}$ yields natural background atmospheric
299 Hg concentrations of 0.2 and 0.4 ng m⁻³ for the NH and SH. In summary, the lower SH enrichment in
300 atmospheric Hg appears to be caused by a combination of lower SH anthropogenic Hg emissions, and
301 higher SH background Hg concentrations. We speculate that the higher SH atmospheric background is
302 driven by a lower SH land/ocean ratio which limits the terrestrial vegetation Hg pump and sustains higher
303 natural marine Hg emissions. Observations and model simulations will need to assess if and when NH
304 Ocean waters, charged with multiple centuries of anthropogenic Hg will resurface in the SH. Overall, our
305 findings suggest that both background Hg concentrations and all-time Hg enrichment in the NH and SH are
306 different and should be taken into account in environmental policy objectives.

307 **Acknowledgements**

308 Field work was funded by the French Polar Institute (IPEV, Brest, France) through the IPEV Programmes
309 1066 "PARAD" (to F.D.V.) and 1065 PALATIO (to N.V.P. and E. Michel). J.E.S. acknowledges funding from
310 the H2020 ERA-PLANET (689443) iGOSP and iCUPE programmes. We thank the South Atlantic
311 Environmental Research Institute (SAERI) for providing laboratory facilities in the Falkland Islands and E.
312 Brook (Falkland Islands Government Training Centre) for logistical support. We are grateful to N. Marchand
313 (IPEV) for the logistical support, C. Marteau for making the sampling possible in very restricted areas of
314 the TAAF Nature Reserve, and N. Roberts for help processing the San Carlos core and scientific discussions.
315 We thank A. Coronato, R. López and V. Pancotto from CADIC-CONICET (Ushuaia) for the field campaigns in
316 Andorra and Harberton. Radiocarbon ages were obtained as part of the IDEX Peat3 project of the University
317 of Toulouse and through the national service support: Artemis-INSU-CNRS (to G.L.R.). C.L.'s PhD is
318 supported by a scholarship from the China Scholarship Council.

319 **Author Contributions**

320 J.E.S and F.D.V initiated and designed the project. All authors were involved in field sampling, laboratory
321 analyses, and/or data analysis. C.L. and J.E.S wrote the manuscript on which all authors commented.

322 **Data availability statement**

323 All data generated or analyzed during this study are included in this published article (and its SI
324 Appendix).

325 **References**

- 326 (1) Outridge, P. M.; Mason, R. P.; Wang, F.; Guerrero, S.; Heimbürger-Boavida, L. E. Updated Global
327 and Oceanic Mercury Budgets for the United Nations Global Mercury Assessment 2018. *Environ.*
328 *Sci. Technol.* **2018**, *52* (20), 11466–11477. <https://doi.org/10.1021/acs.est.8b01246>.
- 329 (2) Mason, R. P.; Choi, A. L.; Fitzgerald, W. F.; Hammerschmidt, C. R.; Lamborg, C. H.; Soerensen, A. L.;
330 Sunderland, E. M. Mercury Biogeochemical Cycling in the Ocean and Policy Implications. *Environ.*
331 *Res.* **2012**, *119*, 101–117. <https://doi.org/10.1016/j.envres.2012.03.013>.
- 332 (3) Chen, C.; Amirbahman, A.; Fisher, N.; Harding, G.; Lamborg, C.; Nacci, D.; Taylor, D.
333 Methylmercury in Marine Ecosystems: Spatial Patterns and Processes of Production,
334 Bioaccumulation, and Biomagnification. *Ecohealth* **2008**, *5* (4), 399–408.
335 <https://doi.org/10.1007/s10393-008-0201-1>.
- 336 (4) Sunderland, E. M. Mercury Exposure from Domestic and Imported Estuarine and Marine Fish in
337 the U.S. Seafood Market. *Environ. Health Perspect.* **2007**, *115* (235–242).
- 338 (5) Pirrone, N.; Cinnirella, S.; Feng, X.; Finkelman, R. B.; Friedli, H. R.; Leaner, J.; Mason, R.;
339 Mukherjee, A. B.; Stracher, G. B.; Streets, D. G.; Telmer, K. Global Mercury Emissions to the
340 Atmosphere from Anthropogenic and Natural Sources. *Atmospheric Chem. Phys.* **2010**, *10* (13),
341 5951–5964. <https://doi.org/10.5194/acp-10-5951-2010>.
- 342 (6) Pacyna, E. G.; Pacyna, J. M.; Sundseth, K.; Munthe, J.; Kindbom, K.; Wilson, S.; Steenhuisen, F.;
343 Maxson, P. Global Emission of Mercury to the Atmosphere from Anthropogenic Sources in 2005
344 and Projections to 2020. *Atmos. Environ.* **2010**, *44* (20), 2487–2499.
345 <https://doi.org/10.1016/j.atmosenv.2009.06.009>.
- 346 (7) Streets, D. G.; Horowitz, H. M.; Jacob, D. J.; Lu, Z.; Levin, L.; ter Schure, A. F. H.; Sunderland, E. M.
347 Total Mercury Released to the Environment by Human Activities. *Environ. Sci. Technol.* **2017**, *51*
348 (11), 5969–5977. <https://doi.org/10.1021/acs.est.7b00451>.
- 349 (8) Horowitz, H. M.; Jacob, D. J.; Zhang, Y.; Dibble, T. S.; Slemr, F.; Amos, H. M.; Schmidt, J. A.; Corbitt,
350 E. S.; Marais, E. A.; Sunderland, E. M. A New Mechanism for Atmospheric Mercury Redox
351 Chemistry: Implications for the Global Mercury Budget. *Atmospheric Chem. Phys.* **2017**, *17* (10),
352 6353–6371. <https://doi.org/10.5194/acp-17-6353-2017>.
- 353 (9) Fitzgerald, W. F.; Engstrom, D. R.; Mason, R. P.; Nater, E. A. The Case for Atmospheric Mercury
354 Contamination in Remote Areas. *Environ. Sci. Technol.* **1998**, *32* (1), 1–7.
355 <https://doi.org/10.1021/es970284w>.
- 356 (10) Engstrom, D. R.; Fitzgerald, W. F.; Cooke, C. A.; Lamborg, C. H.; Drevnick, P. E.; Swain, E. B.;
357 Balogh, S. J.; Balcom, P. H. Atmospheric Hg Emissions from Preindustrial Gold and Silver Extraction
358 in the Americas: A Reevaluation from Lake-Sediment Archives. *Environ. Sci. Technol.* **2014**, *48* (12),
359 6533–6543. <https://doi.org/10.1021/es405558e>.

- 360 (11) Martınez-Cortizas, A. Mercury in a Spanish Peat Bog: Archive of Climate Change and
 361 Atmospheric Metal Deposition. *Science* **1999**, *284* (5416), 939–942.
 362 <https://doi.org/10.1126/science.284.5416.939>.
- 363 (12) Schuster, P. F.; Krabbenhoft, D. P.; Naftz, D. L.; Cecil, L. D.; Olson, M. L.; Dewild, J. F.; Susong, D. D.;
 364 Green, J. R.; Abbott, M. L. Atmospheric Mercury Deposition during the Last 270 Years: A Glacial
 365 Ice Core Record of Natural and Anthropogenic Sources. *Environ. Sci. Technol.* **2002**, *36* (11), 2303–
 366 2310. <https://doi.org/10.1021/es0157503>.
- 367 (13) Thomas, R. L. The Distribution of Mercury in the Sediments of Lake Ontario. *Can. J. Earth Sci.*
 368 **1972**, *9* (6), 636–651. <https://doi.org/10.1139/e72-054>.
- 369 (14) UNEP. *Global Mercury Assessment 2018*; 2018.
- 370 (15) Biester, H.; Bindler, R.; Martinez-Cortizas, A.; Engstrom, D. R. Modeling the Past Atmospheric
 371 Deposition of Mercury Using Natural Archives. *Environ. Sci. Technol.* **2007**, *41* (14), 4851–4860.
 372 <https://doi.org/10.1021/es0704232>.
- 373 (16) Amos, H. M.; Sonke, J. E.; Obrist, D.; Robins, N.; Hagan, N.; Horowitz, H. M.; Mason, R. P.; Witt, M.;
 374 Hedgecock, I. M.; Corbitt, E. S.; Sunderland, E. M. Observational and Modeling Constraints on
 375 Global Anthropogenic Enrichment of Mercury. *Environ. Sci. Technol.* **2015**, *49* (7), 4036–4047.
 376 <https://doi.org/10.1021/es5058665>.
- 377 (17) Zhang, Y.; Jaeglé, L.; Thompson, L.; Streets, D. G. Six Centuries of Changing Oceanic Mercury:
 378 Anthropogenic Mercury in Ocean. *Glob. Biogeochem. Cycles* **2014**, *28* (11), 1251–1261.
 379 <https://doi.org/10.1002/2014GB004939>.
- 380 (18) Biester, H.; Bindler, R.; Martinez-Cortizas, A.; Engstrom, D. R. Modeling the Past Atmospheric
 381 Deposition of Mercury Using Natural Archives. *Environ. Sci. Technol.* **2007**, *41* (14), 4851–4860.
 382 <https://doi.org/10.1021/es0704232>.
- 383 (19) Cooke, C. A.; Hobbs, W. O.; Michelutti, N.; Wolfe, A. P. Reliance on Pb-210 Chronology Can
 384 Compromise the Inference of Preindustrial Hg Flux to Lake Sediments. *Environ. Sci. Technol.* **2010**,
 385 *44* (6), 1998–2003. <https://doi.org/10.1021/es9027925>.
- 386 (20) Abril, J. M.; Brunskill, G. Evidence That Excess 210Pb Flux Varies with Sediment Accumulation Rate
 387 and Implications for Dating Recent Sediments. *J. Paleolimnol.* **2014**, *52*.
 388 <https://doi.org/10.1007/s10933-014-9782-6>.
- 389 (21) Enrico, M.; Roux, G. L.; Maruszczak, N.; Heimbürger, L.-E.; Claustres, A.; Fu, X.; Sun, R.; Sonke, J. E.
 390 Atmospheric Mercury Transfer to Peat Bogs Dominated by Gaseous Elemental Mercury Dry
 391 Deposition. *Environ. Sci. Technol.* **2016**, *50* (5), 2405–2412.
 392 <https://doi.org/10.1021/acs.est.5b06058>.
- 393 (22) Jiskra, M.; Sonke, J. E.; Obrist, D.; Bieser, J.; Ebinghaus, R.; Myhre, C. L.; Pfaffhuber, K. A.;
 394 Wängberg, I.; Kyllönen, K.; Worthy, D.; Martin, L. G.; Labuschagne, C.; Mkololo, T.; Ramonet, M.;
 395 Magand, O.; Dommergue, A. A Vegetation Control on Seasonal Variations in Global Atmospheric
 396 Mercury Concentrations. *Nat. Geosci.* **2018**, *11* (4), 244–250. <https://doi.org/10.1038/s41561-018-0078-8>.
- 398 (23) Enrico, M.; Le Roux, G.; Heimbürger, L.-E.; Van Beek, P.; Souhaut, M.; Chmeleff, J.; Sonke, J. E.
 399 Holocene Atmospheric Mercury Levels Reconstructed from Peat Bog Mercury Stable Isotopes.
 400 *Environ. Sci. Technol.* **2017**, *51* (11), 5899–5906. <https://doi.org/10.1021/acs.est.6b05804>.
- 401 (24) European Monitoring and Evaluation Programme. <https://www.emep.int/> 2016.
- 402 (25) Streets, D. G.; Devane, M. K.; Lu, Z.; Bond, T. C.; Sunderland, E. M.; Jacob, D. J. All-Time Releases
 403 of Mercury to the Atmosphere from Human Activities. *Environ. Sci. Technol.* **2011**, *45* (24), 10485–
 404 10491. <https://doi.org/10.1021/es202765m>.
- 405 (26) Streets, D. G.; Horowitz, H. M.; Lu, Z.; Levin, L.; Thackray, C. P.; Sunderland, E. M. Five Hundred
 406 Years of Anthropogenic Mercury: Spatial and Temporal Release Profiles. *Environ. Res. Lett.* **2019**,
 407 *14* (8), 084004. <https://doi.org/10.1088/1748-9326/ab281f>.

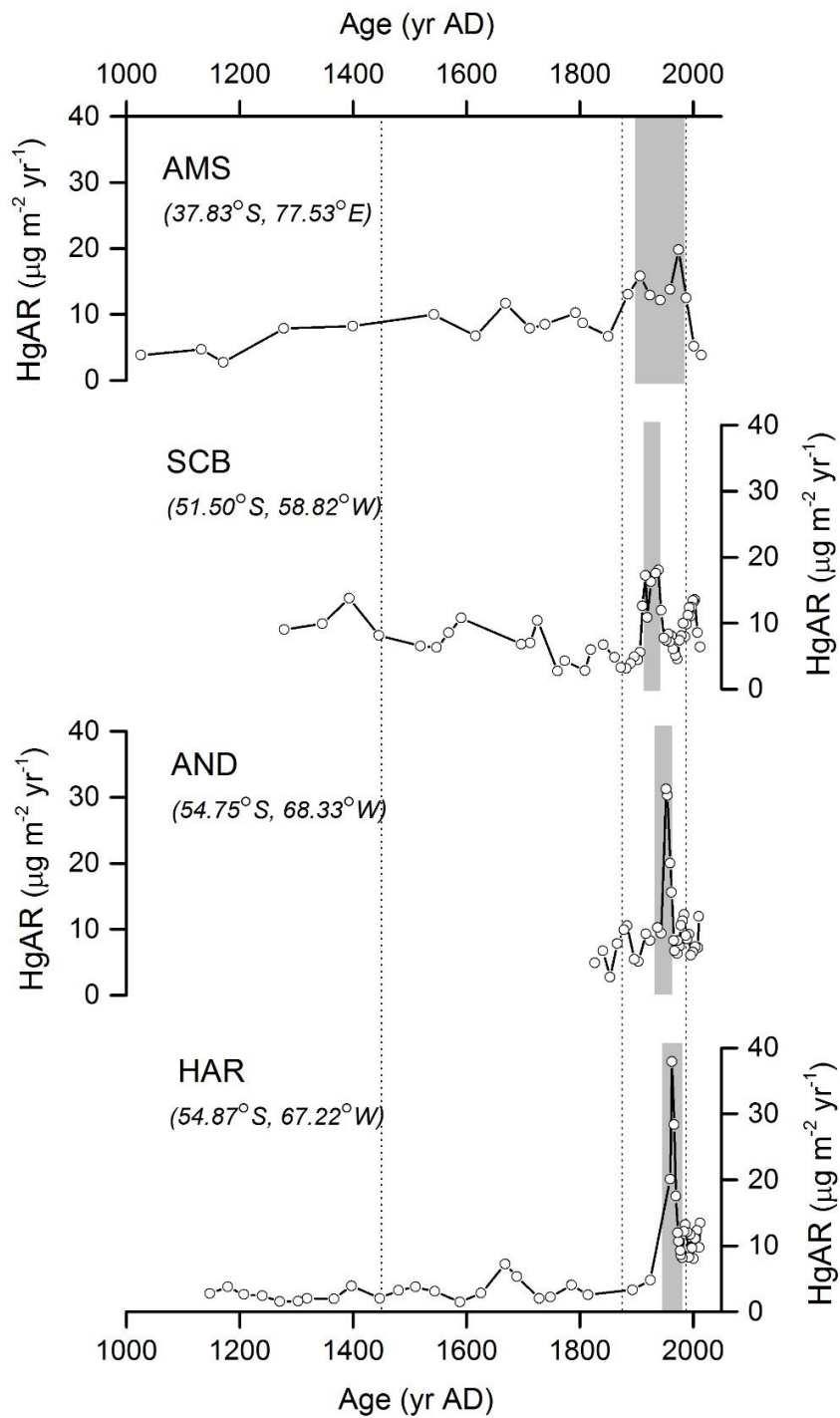
- 408 (27) Amos, H. M.; Jacob, D. J.; Streets, D. G.; Sunderland, E. M. Legacy Impacts of All-Time
 409 Anthropogenic Emissions on the Global Mercury Cycle: GLOBAL IMPACTS OF LEGACY MERCURY.
 410 *Glob. Biogeochem. Cycles* **2013**, *27* (2), 410–421. <https://doi.org/10.1002/gbc.20040>.
- 411 (28) Engstrom, D. R.; Fitzgerald, W. F.; Cooke, C. A.; Lamborg, C. H.; Drevnick, P. E.; Swain, E. B.;
 412 Balogh, S. J.; Balcom, P. H. Atmospheric Hg Emissions from Preindustrial Gold and Silver Extraction
 413 in the Americas: A Reevaluation from Lake-Sediment Archives. *Environ. Sci. Technol.* **2014**, *48* (12),
 414 6533–6543. <https://doi.org/10.1021/es405558e>.
- 415 (29) Cooke, C. A.; Hintelmann, H.; Ague, J. J.; Burger, R.; Biester, H.; Sachs, J. P.; Engstrom, D. R. Use
 416 and Legacy of Mercury in the Andes. *Environ. Sci. Technol.* **2013**, *47* (9), 4181–4188.
 417 <https://doi.org/10.1021/es3048027>.
- 418 (30) Streets, D. G.; Horowitz, H. M.; Jacob, D.; Lu, Z.; Levin, L.; ter Schure, A. F. H.; Sunderland, E. M.
 419 Total Mercury Released to the Environment by Human Activities. *Environ. Sci. Technol.* **2017**, *51*
 420 (11), 5969–5977. <https://doi.org/10.1021/acs.est.7b00451>.
- 421 (31) Amos, H. M.; Sonke, J. E.; Obrist, D.; Robins, N.; Hagan, N.; Horowitz, H. M.; Mason, R. P.; Witt, M.;
 422 Hedgecock, I. M.; Corbitt, E. S.; Sunderland, E. M. Observational and Modeling Constraints on
 423 Global Anthropogenic Enrichment of Mercury. *Environ. Sci. Technol.* **2015**, *49* (7), 4036–4047.
 424 <https://doi.org/10.1021/es5058665>.
- 425 (32) Cooke, C. A.; Martínez-Cortizas, A.; Bindler, R.; Gustin, M. S. Environmental Archives of
 426 Atmospheric Hg Deposition – A Review. *Sci. Total Environ.* **2020**, *709*, 134800.
 427 <https://doi.org/https://doi.org/10.1016/j.scitotenv.2019.134800>.
- 428 (33) Lindberg, S.; Bullock, R.; Ebinghaus, R.; Engstrom, D.; Feng, X.; Fitzgerald, W.; Pirrone, N.; Prestbo,
 429 E.; Seigneur, C. A Synthesis of Progress and Uncertainties in Attributing the Sources of Mercury
 430 Deposition. *Ambio* **2007**, *36*, 19–32.
- 431 (34) Biester, H.; Kilian, R.; Franzen, C.; Woda, C.; Mangini, A.; Schöler, H. F. Elevated Mercury
 432 Accumulation in a Peat Bog of the Magellanic Moorlands, Chile (53°S) – an Anthropogenic Signal
 433 from the Southern Hemisphere. *Earth Planet. Sci. Lett.* **2002**, *201* (3–4), 609–620.
 434 [https://doi.org/10.1016/S0012-821X\(02\)00734-3](https://doi.org/10.1016/S0012-821X(02)00734-3).
- 435 (35) Guédron, S.; Ledru, M.-P.; Escobar-Torrez, K.; Develle, A. L.; Brisset, E. Enhanced Mercury
 436 Deposition by Amazonian Orographic Precipitation: Evidence from High-Elevation Holocene
 437 Records of the Lake Titicaca Region (Bolivia). *Palaeogeogr. Palaeoclimatol. Palaeoecol.* **2018**, *511*,
 438 577–587. <https://doi.org/10.1016/j.palaeo.2018.09.023>.
- 439 (36) Le Roux, G.; Vleeschouwer, F. Preparation of Peat Samples for Inorganic Geochemistry Used as
 440 Palaeoenvironmental Proxies. *Mires Peat* **2011**, *7*.
- 441 (37) Givélet, N.; Le Roux, G.; Cheburkin, A.; Chen, B.; Frank, J.; Goodsite, M.; Kempter, H.; Krachler, M.;
 442 Noernberg, T.; Rausch, N.; Rheinberger, S.; Roos-Barraclough, F.; Sapkota, A.; Scholz, C.; Shotyk,
 443 W. Suggested Protocol for Collecting, Handling and Preparing Peat Cores and Peat Samples for
 444 Physical, Chemical, Mineralogical and Isotopic Analyses. *J. Environ. Monit.* **2004**, *6* (5), 481–492.
 445 <https://doi.org/10.1039/b401601g>.
- 446 (38) Li, C., Sonke, J.E., Le Roux, G., Van der Putten, N., Piotrowska, N., Jeandel C., Mattielli N., Benoit
 447 M., Wiggs G.F.S., & De Vleeschouwer. Holocene Dynamics of the Southern Hemisphere Westerly
 448 Winds over the Indian Ocean Inferred from a Peat Dust Deposition Record. *Under review in*
 449 *Quaternary Science Reviews*.
- 450 (39) Goodsite, M. E.; Rom, W.; Heinemeier, J.; Lange, T.; Ooi, S.; Appleby, P. G.; Shotyk, W.; van der
 451 Knaap, W. O.; Lohse, C.; Hansen, T. S. High-Resolution AMS ¹⁴C Dating of Post-Bomb Peat Archives
 452 of Atmospheric Pollutants. *Radiocarbon* **2001**, *43* (2B), 495–515.
 453 <https://doi.org/10.1017/S0033822200041163>.

- 454 (40) Appleby, P. G. Chronostratigraphic Techniques in Recent Sediments. In *Tracking Environmental*
455 *Change Using Lake Sediments*; Last, W. M., Smol, J. P., Eds.; Kluwer Academic Publishers:
456 Dordrecht, 2002; Vol. 1, pp 171–203. https://doi.org/10.1007/0-306-47669-X_9.
- 457 (41) Piotrowska, N. Status Report of AMS Sample Preparation Laboratory at GADAM Centre, Gliwice,
458 Poland. *Nucl. Instrum. Methods Phys. Res. Sect. B Beam Interact. Mater. At.* **2013**, *294*, 176–181.
459 <https://doi.org/10.1016/j.nimb.2012.05.017>.
- 460 (42) Zoppi, U.; Crye, J.; Song, Q.; Arjomand, A. Performance Evaluation of the New AMS System at
461 Accium BioSciences. *Radiocarbon* **2007**, *49* (1), 171–180.
462 <https://doi.org/10.1017/S0033822200041990>.
- 463 (43) Davies, L. J.; Appleby, P.; Jensen, B. J. L.; Magnan, G.; Mullan-Boudreau, G.; Noernberg, T.;
464 Shannon, B.; Shotyk, W.; van Bellen, S.; Zaccone, C.; Froese, D. G. High-Resolution Age Modelling
465 of Peat Bogs from Northern Alberta, Canada, Using Pre- and Post-Bomb ¹⁴C, ²¹⁰Pb and Historical
466 Cryptotephra. *Quat. Geochronol.* **2018**, *47*, 138–162.
467 <https://doi.org/10.1016/j.quageo.2018.04.008>.
- 468 (44) Blaauw, M.; Christen, J. A. Flexible Paleoclimate Age-Depth Models Using an Autoregressive
469 Gamma Process. *Bayesian Anal.* **2011**, *6* (3), 457–474. <https://doi.org/10.1214/11-BA618>.
- 470 (45) Hogg, A. G.; Hua, Q.; Blackwell, P. G.; Niu, M.; Buck, C. E.; Guilderson, T. P.; Heaton, T. J.; Palmer, J.
471 G.; Reimer, P. J.; Reimer, R. W.; Turney, C. S. M.; Zimmerman, S. R. H. SHCal13 Southern
472 Hemisphere Calibration, 0–50,000 Years Cal BP. *Radiocarbon* **2013**, *55* (4), 1889–1903.
473 https://doi.org/10.2458/azu_js_rc.55.16783.
- 474 (46) Hua, Q.; Barbetti, M.; Rakowski, A. Z. Atmospheric Radiocarbon for the Period 1950–2010.
475 *Radiocarbon* **2013**, *55* (4), 2059–2072. https://doi.org/10.2458/azu_js_rc.v55i2.16177.
- 476 (47) Lamborg, C. H.; Fitzgerald, W. F.; Damman, A. W. H.; Benoit, J. M.; Balcom, P. H.; Engstrom, D. R.
477 Modern and Historic Atmospheric Mercury Fluxes in Both Hemispheres: Global and Regional
478 Mercury Cycling Implications: MODERN AND HISTORIC FLUXES OF ATMOSPHERIC MERCURY. *Glob.*
479 *Biogeochem. Cycles* **2002**, *16* (4), 51-1-51–11. <https://doi.org/10.1029/2001GB001847>.
- 480 (48) Cooke, C. A.; Balcom, P. H.; Kerfoot, C.; Abbott, M. B.; Wolfe, A. P. Pre-Colombian Mercury
481 Pollution Associated with the Smelting of Argentiferous Ores in the Bolivian Andes. *AMBIO* **2011**,
482 *40* (1), 18–25. <https://doi.org/10.1007/s13280-010-0086-4>.
- 483 (49) Ribeiro Guevara, S.; Meili, M.; Rizzo, A.; Daga, R.; Arribére, M. Sediment Records of Highly
484 Variable Mercury Inputs to Mountain Lakes in Patagonia during the Past Millennium. *Atmospheric*
485 *Chem. Phys.* **2010**, *10* (7), 3443–3453. <https://doi.org/10.5194/acp-10-3443-2010>.
- 486 (50) Cooke, C. A.; Balcom, P. H.; Biester, H.; Wolfe, A. P. Over Three Millennia of Mercury Pollution in
487 the Peruvian Andes. *Proc. Natl. Acad. Sci.* **2009**, *106* (22), 8830–8834.
488 <https://doi.org/10.1073/pnas.0900517106>.
- 489 (51) Guerero, S. Chemistry as a Tool for Historical Research: Identifying Paths of Historical Mercury
490 Pollution in the Hispanic New World. *Bull Hist Chem* **2012**, *37*, 61–70.
- 491 (52) Saiz-Lopez, A.; Sitkiewicz, S. P.; Roca-Sanjuán, D.; Oliva-Enrich, J. M.; Dávalos, J. Z.; Notario, R.;
492 Jiskra, M.; Xu, Y.; Wang, F.; Thackray, C. P.; Sunderland, E. M.; Jacob, D. J.; Travníkov, O.; Cuevas,
493 C. A.; Acuña, A. U.; Rivero, D.; Plane, J. M. C.; Kinnison, D. E.; Sonke, J. E. Photoreduction of
494 Gaseous Oxidized Mercury Changes Global Atmospheric Mercury Speciation, Transport and
495 Deposition. *Nat. Commun.* **2018**, *9* (1), 4796. <https://doi.org/10.1038/s41467-018-07075-3>.
- 496 (53) Bagnato, E.; Tamburello, G.; Avard, G.; Martínez-Cruz, M.; Enrico, M.; Fu, X.; Sprovieri, M.; Sonke,
497 J. E. Mercury Fluxes from Volcanic and Geothermal Sources: An Update. *Geol. Soc. Lond. Spec.*
498 *Publ.* **2015**, *410* (1), 263–285. <https://doi.org/10.1144/SP410.2>.
- 499 (54) Andres, R. J.; Kasgnoc, A. D. A Time-Averaged Inventory of Subaerial Volcanic Sulfur Emissions. *J.*
500 *Geophys. Res. Atmospheres* **1998**, *103* (D19), 25251–25261. <https://doi.org/10.1029/98JD02091>.

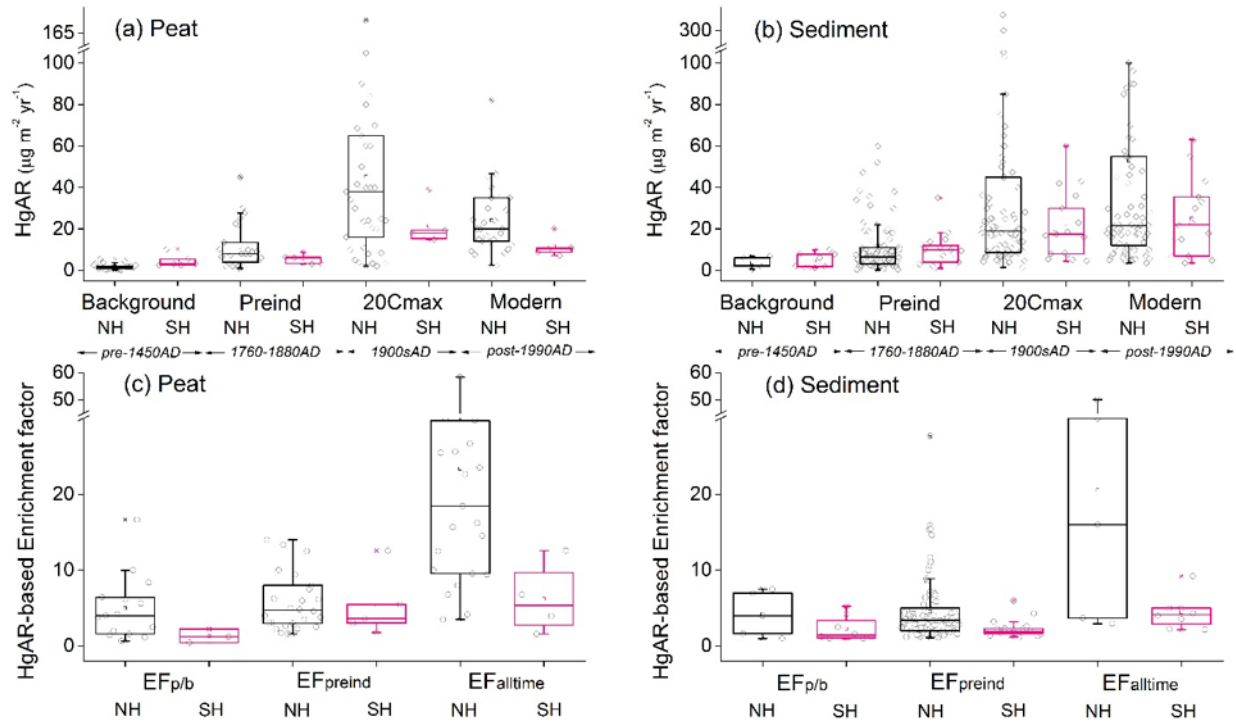
- 501 (55) Carn, S. A.; Fioletov, V. E.; McLinden, C. A.; Li, C.; Krotkov, N. A. A Decade of Global Volcanic SO₂
502 Emissions Measured from Space. *Sci. Rep.* **2017**, *7* (1), 44095. <https://doi.org/10.1038/srep44095>.
- 503 (56) Kocman, D.; Horvat, M.; Pirrone, N.; Cinnirella, S. Contribution of Contaminated Sites to the
504 Global Mercury Budget. *Environ. Res.* **2013**, *125*, 160–170.
505 <https://doi.org/10.1016/j.envres.2012.12.011>.
- 506 (57) Agnan, Y.; Le Dantec, T.; Moore, C. W.; Edwards, G. C.; Obrist, D. New Constraints on Terrestrial
507 Surface–Atmosphere Fluxes of Gaseous Elemental Mercury Using a Global Database. *Environ. Sci.*
508 *Technol.* **2016**, *50* (2), 507–524. <https://doi.org/10.1021/acs.est.5b04013>.
- 509 (58) Fitzgerald, W.F. and Lamborg, C.H.,. Geochemistry of Mercury. Treatise on Geochemistry: Volume
510 9: Environmental Geochemistry; 2004.
- 511 (59) Lamborg, C. H.; Von Damm, K. L.; Fitzgerald, W. F.; Hammerschmidt, C. R.; Zierenberg, R. Mercury
512 and Methylmercury in Fluids from Sea Cliff Submarine Hydrothermal Field, Gorda Ridge.
513 *Geophys. Res. Lett.* **2006**, *33* (17), L17606. <https://doi.org/10.1029/2006GL026321>.
- 514 (60) Bowman, K. L.; Hammerschmidt, C. R.; Lamborg, C. H.; Swarr, G. J.; Agather, A. M. Distribution of
515 Mercury Species across a Zonal Section of the Eastern Tropical South Pacific Ocean (U.S.
516 GEOTRACES GP16). *Mar. Chem.* **2016**, *186*, 156–166.
517 <https://doi.org/10.1016/j.marchem.2016.09.005>.
- 518 (61) Demers, J. D.; Blum, J. D.; Zak, D. R. Mercury Isotopes in a Forested Ecosystem: Implications for
519 Air-Surface Exchange Dynamics and the Global Mercury Cycle. *Glob. Biogeochem. Cycles* **2013**, *27*
520 (1), 222–238. <https://doi.org/10.1002/gbc.20021>.
- 521 (62) Enrico, M.; Le Roux, G.; Maruszczak, N.; Heimbürger, L.-E.; Claustres, A.; Fu, X.; Sun, R.; Sonke, J. E.
522 Atmospheric Mercury Transfer to Peat Bogs Dominated by Gaseous Elemental Mercury Dry
523 Deposition. *Environ. Sci. Technol.* **2016**. <https://doi.org/10.1021/acs.est.5b06058>.
- 524 (63) Enrico, M.; Le Roux, G.; Heimbürger, L.-E.; Van Beek, P.; Souhaut, M.; Chmeleff, J.; Sonke, J. E.
525 Holocene Atmospheric Mercury Levels Reconstructed from Peat Bog Mercury Stable Isotopes.
526 *Environ. Sci. Technol.* **2017**, *51* (11), 5899–5906. <https://doi.org/10.1021/acs.est6b05804>.
- 527 (64) Zheng, W.; Obrist, D.; Weis, D.; Bergquist, B. A. Mercury Isotope Compositions across North
528 American Forests. *Glob. Biogeochem. Cycles* **2016**, *30* (10), 1475–1492.
529 <https://doi.org/10.1002/2015GB005323>.
- 530 (65) Slemr, F.; Seiler, W.; Schuster, G. Latitudinal Distribution of Mercury over the Atlantic Ocean. *J.*
531 *Geophys. Res.* **1981**, *86* (C2), 1159. <https://doi.org/10.1029/JC086iC02p01159>.
- 532 (66) Bieser, J.; Slemr, F.; Ambrose, J.; Brenninkmeijer, C.; Brooks, S.; Dastoor, A.; DeSimone, F.;
533 Ebinghaus, R.; Gencarelli, C. N.; Geyer, B.; Gratz, L. E.; Hedgecock, I. M.; Jaffe, D.; Kelley, P.; Lin, C.-
534 J.; Jaegle, L.; Matthias, V.; Ryjkov, A.; Selin, N. E.; Song, S.; Travnikov, O.; Weigelt, A.; Luke, W.;
535 Ren, X.; Zahn, A.; Yang, X.; Zhu, Y.; Pirrone, N. Multi-Model Study of Mercury Dispersion in the
536 Atmosphere: Vertical and Interhemispheric Distribution of Mercury Species. *Atmospheric Chem.*
537 *Phys.* **2017**, *17* (11), 6925–6955. <https://doi.org/10.5194/acp-17-6925-2017>.
- 538 (67) Sprovieri, F.; Pirrone, N.; Bencardino, M.; D'Amore, F.; Carbone, F.; Cinnirella, S.;
539 Mannarino, V.; Landis, M.; Ebinghaus, R.; Weigelt, A.; Brunke, E.-G.; Labuschagne, C.; Martin, L.;
540 Munthe, J.; Wängberg, I.; Artaxo, P.; Morais, F.; Barbosa, H. de M. J.; Brito, J.; Cairns, W.;
541 Barbante, C.; Diéguez, M. del C.; Garcia, P. E.; Dommergue, A.; Angot, H.; Magand, O.; Skov, H.;
542 Horvat, M.; Kotnik, J.; Read, K. A.; Neves, L. M.; Gawlik, B. M.; Sena, F.; Mashyanov, N.; Obolkin,
543 V.; Wip, D.; Feng, X. B.; Zhang, H.; Fu, X.; Ramachandran, R.; Cossa, D.; Knoery, J.; Maruszczak, N.;
544 Nerentorp, M.; Norstrom, C. Atmospheric Mercury Concentrations Observed at Ground-Based
545 Monitoring Sites Globally Distributed in the Framework of the GMOS Network. *Atmospheric*
546 *Chem. Phys.* **2016**, *16* (18), 11915–11935. <https://doi.org/10.5194/acp-16-11915-2016>.
- 547 (68) Zhang, Y.; Jacob, D. J.; Horowitz, H. M.; Chen, L.; Amos, H. M.; Krabbenhoft, D. P.; Slemr, F.; St.
548 Louis, V. L.; Sunderland, E. M. Observed Decrease in Atmospheric Mercury Explained by Global

- 549 Decline in Anthropogenic Emissions. *Proc. Natl. Acad. Sci.* **2016**, *113* (3), 526–531.
550 <https://doi.org/10.1073/pnas.1516312113>.
- 551 (69) Strode, S. A.; Jaeglé, L.; Selin, N. E.; Jacob, D. J.; Park, R. J.; Yantosca, R. M.; Mason, R. P.; Slemr, F.
552 Air-Sea Exchange in the Global Mercury Cycle: MERCURY AIR-SEA EXCHANGE. *Glob. Biogeochem.*
553 *Cycles* **2007**, *21* (1). <https://doi.org/10.1029/2006GB002766>.
- 554 (70) Bieser, J.; Angot, H.; Slemr, F.; Martin, L. *Atmospheric Mercury in the Southern Hemisphere*
555 *– Part 2: Source Apportionment Analysis at Cape Point Station, South Africa*; preprint;
556 Gases/Field Measurements/Troposphere/Chemistry (chemical composition and reactions), 2020.
557 <https://doi.org/10.5194/acp-2020-63>.
558
559

560 **Figures**
561



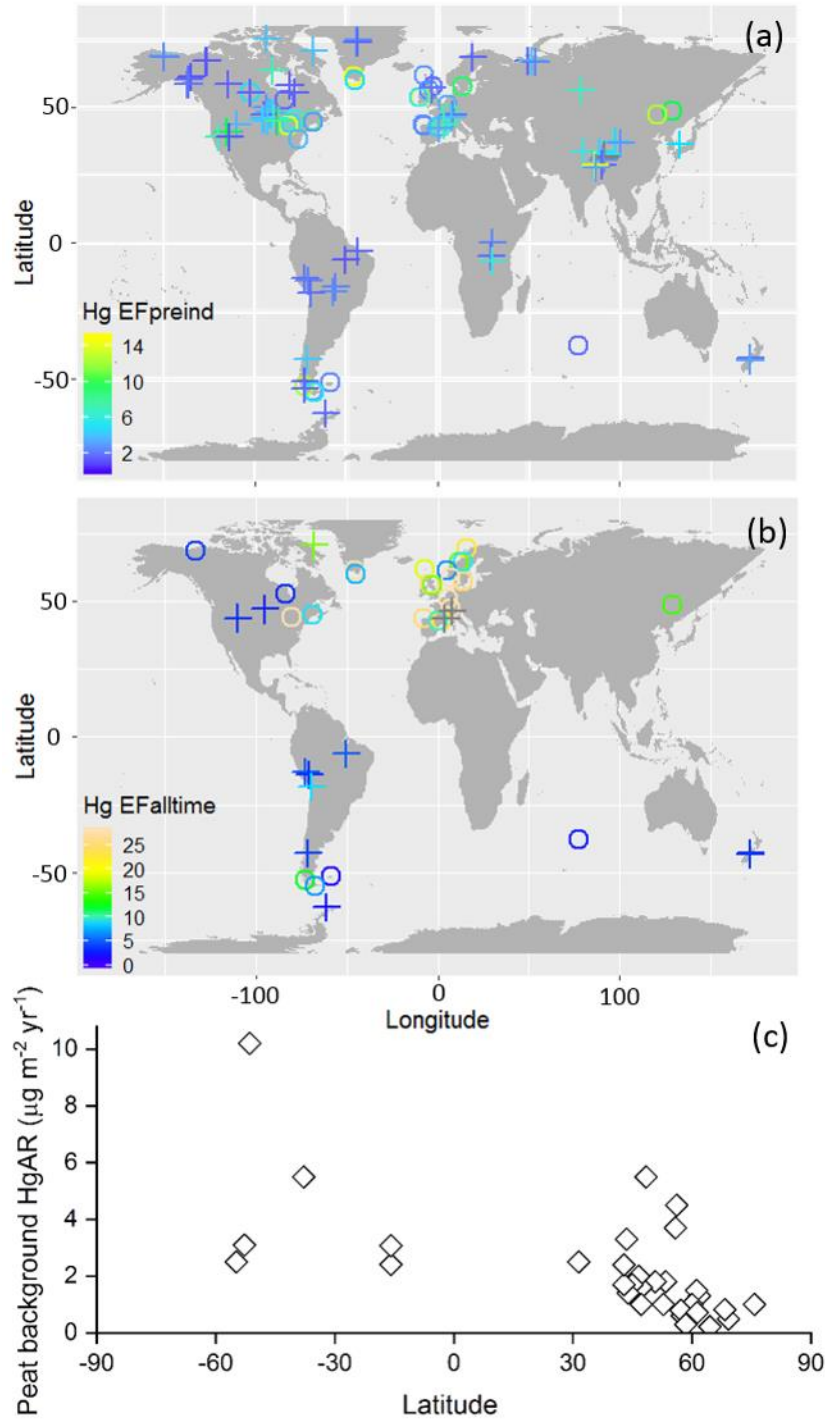
562
563 Figure 1. Profiles of Hg accumulation rates (HgAR) in the peat cores from Amsterdam Island (AMS), Falkland
564 Islands (SCB, Islas Malvinas), Andorra and Harberton (AND, HAR, Tierra del Fuego). Vertical dashed lines
565 operationally separate the natural background (pre-1450AD), pre-industrial (1450-1880AD), the extended
566 20th century maximum HgAR (20Cmax, grey bars) and modern (post-1990AD) reference periods, following
567 reference ¹⁵).



568

569 Figure 2. Review of published Hg accumulation rates (HgAR) and enrichment factors (EF) in NH and SH peat
 570 and sediment cores for different reference time periods. HgAR ($\mu\text{g m}^{-2} \text{yr}^{-1}$) and EF in peat (A), (C) and
 571 sediment (B), (D) profiles during different periods: Natural background (pre-1450AD), pre-industrial (1450-
 572 1880AD), extended 20th century maximum (20Cmax, defined as the broad 20th century HgAR peak, and
 573 modern period (post-1990AD). $\text{EF}_{\text{p/b}}$: EF from natural background to pre-industrial period. $\text{EF}_{\text{preind}}$: EF from
 574 pre-industrial to 20Cmax. $\text{EF}_{\text{alltime}}$: EF from natural background to 20Cmax.

575



576
 577 Figure 3. Hg enrichment factors between different reference time periods and peat background Hg
 578 accumulation rate. Enrichment factors (EF) in Hg accumulation rates for A) 20th century industrial relative
 579 to pre-industrial periods (EF_{pre-ind}, 1450-1880AD). B) 20th century industrial relative to natural background
 580 periods (EF_{alltime}, pre-1450AD century). Circles represent peat cores, and crosses sediment cores. C) Natural
 581 background Hg accumulation rate (pre-1450AD HgAR) in peat cores as a function of latitude. For details
 582 see Extended Data 2.

583 **Table 1. Hg accumulation rate (HgAR) enrichment factor observed in the peat profiles from this study.**
 584 AMS, Amsterdam Island; SCB, the Falkland Islands; AND, HAR, Andorra and Harberton, Argentina. 'Pre-ind',
 585 pre-industrial; '20Cmax', extended 20th century maximum HgAR (see Methods); 'p/b', pre-
 586 industrial/background.

	Pre-ind/ background (EF _{p/b})	20Cmax/Pre-ind (EF _{Preind})	20Cmax/background (EF _{Alltime})
AMS	1.6	1.7	2.7
SCB	0.6	2.5	1.5
AND		3.0	
HAR	1.4	5.3	7.3

587
 588 **Table 2. Summary of Hg accumulation rate (HgAR) enrichment factors (EF) in global peat and sediment**
 589 **records.** 'Pre-ind', pre-industrial; '20Cmax', extended 20th century maximum HgAR (see Methods); 'p/b',
 590 pre-industrial/background; 'modern/back', 'modern/background'; NH, northern hemisphere; SH,
 591 southern hemisphere.

	Pre-ind /background (EF _{p/b})		20Cmax/pre-ind (EF _{Preind})		20Cmax/background (EF _{alltime})		Modern/ background (EF _{modern/back})	
Global-sediment	1.6	n=13	2.9	n=103	4.3	n=14	5.0	n=10
Global-peat	2.5	n=17	4.3	n=30	14.5	n=25	10.3	n=18
NH-sediment+peat	3.9	n=18	3.3	n=110	16.1	n=26	10.5	n=17
SH-sediment+peat	1.3	n=11	1.9	n=21	4.0	n=13	3.5	n=11
NH-sediment	3.7	n=5	3.1	n=84	12.8	n=5	19.3	n=4
NH-peat	3.9	n=14	4.6	n=25	16.2	n=21	12.3	n=14
SH-sediment	1.4	n=8	1.8	n=17	3.8	n=97	5.0	n=8
SH-peat	1.2	n=3	3.1	n=4	6.0	n=4	3.1	n=4

592 ¹the number of records, n, do not always add up due to the 2 σ outlier tests applied, for ex. SH sediment,
 593 n=8, SH peat, n=3, but SH sediment+peat, n=10. See Methods and Extended Data 2 for details on outlier
 594 tests.

595 **Table 3. Summary of natural and anthropogenic Hg emissions to the atmosphere (mean \pm 1 σ)**

	NH	1 σ	SH	1 σ
passive volcanic degassing (this study) Mg y ⁻¹	92	20	87	19
eruptive volcanic degassing (this study) Mg y ⁻¹	10	10	10	10
crustal degassing ^{56,57} Mg y ⁻¹	91	27	44	13
anthropogenic 20Cmax emissions ⁷ Mg y ⁻¹	2000	500	480	20
Mean EF _{emission}	11.2	4.6	4.4	1.5
Median EF _{alltime}	16.1	10-30 IQR	4.0	2-6 IQR

596
 597

598
599

600 **Supporting Information**

601

602 Unequal anthropogenic enrichment of mercury in Earth's northern and
603 southern hemispheres.

604 Chuxian Li^{1,2}, Jeroen E. Sonke^{2§}, Gaël Le Roux¹, Natalia Piotrowska³, Nathalie Van der Putten⁴,
605 Stephen J. Roberts⁵, Tim Daley⁶, Emma Rice⁶, Roland Gehrels⁷, Maxime Enrico^{1,2,8}, Dmitri
606 Mauquoy⁹, Thomas P. Roland¹⁰, François De Vleeschouwer¹¹

607 *1. EcoLab, Université de Toulouse, CNRS, INPT, UPS, Toulouse, France.*

608 *2. Laboratoire Géosciences Environnement Toulouse, Université de Toulouse, CNRS, IRD, UPS, Toulouse, France.*

609 *3. Silesian University of Technology, Institute of Physics-CSE, Gliwice, Poland.*

610 *4. Faculty of Science, Vrije Universiteit Amsterdam, the Netherlands.*

611 *5. British Antarctic Survey, Cambridge, UK*

612 *6. School of Geography, Earth and Environmental Sciences, Plymouth University, Plymouth PL4 8AA, UK*

613 *7. Department of Environment & Geography, University of York, Heslington, York YO10 5NG, UK*

614 *8. Harvard John A. Paulson School of Engineering & Applied Sciences, Harvard University, Cambridge, MA, USA*

615 *9. Geography and Environment, School of Geosciences, University of Aberdeen, St Mary's Building, Aberdeen, AB24*
616 *3UF, UK*

617 *10. Geography, College of Life and Environmental Sciences, University of Exeter, UK*

618 *11. Instituto Franco-Argentino para el Estudio delClima y sus Impactos (UMI 3351 IFAECI/CNRS-CONICET-UBA),*
619 *Universidad de Buenos Aires, Argentina*

620

621 § Corresponding author: jeroen.sonke@get.omp.eu

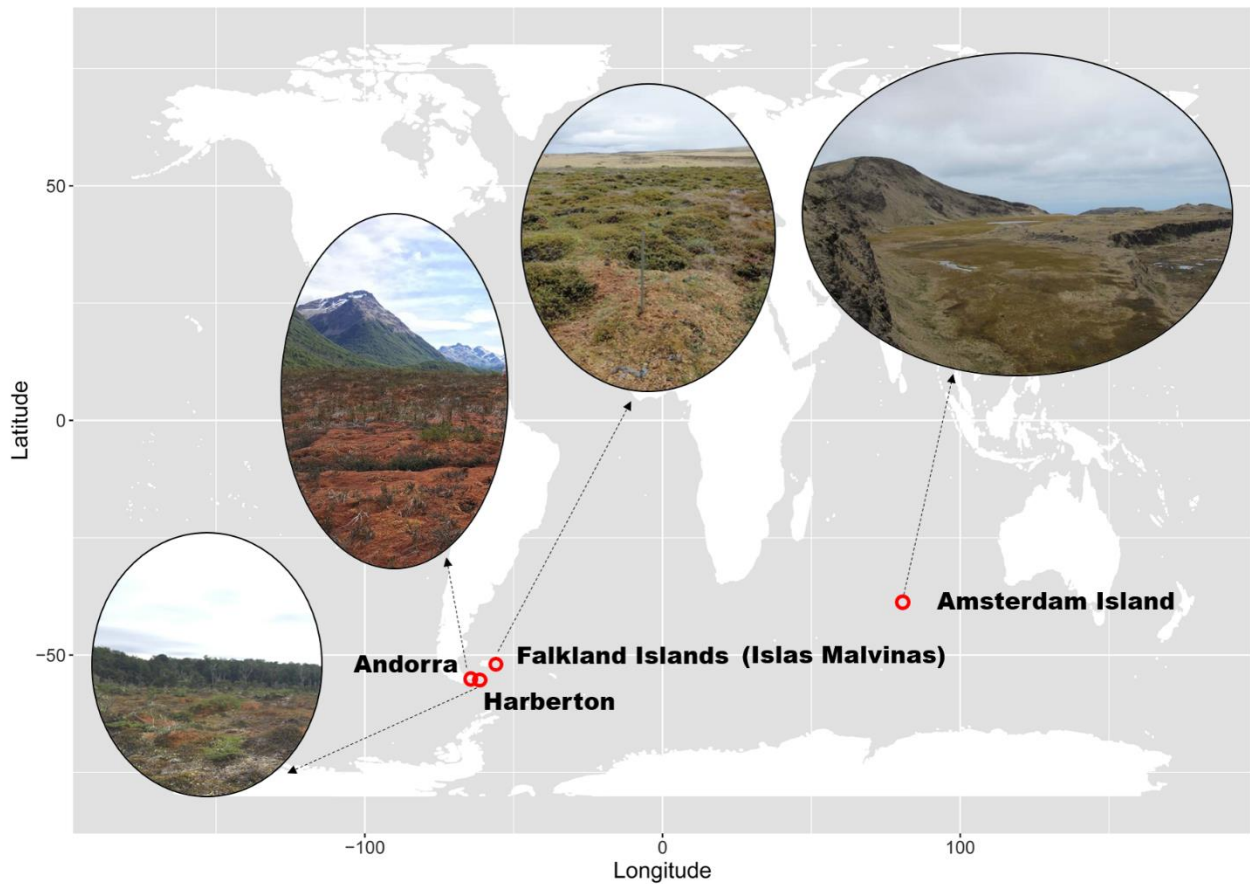
622 This SI contains Table S1, S2, Text S1, Figures S1, S2, S3, S4, S5, S6.

623

624 **Table S1. Details of the coring sites in this investigation**

Location	Site name	coordinates	Elevation (m a.s.l)	Precipitation (mm yr ⁻¹)	Coring date	Label core	core length (m)
Amsterdam Island	Central plateau	37.83°S, 77.53°E	738	1124	11/2014	AMS14-PB01	5
Falkland Islands (Islas Malvinas)	San Carlos bog	51.50°S, 58.82°W	8	575	2013	SCB13-PB01C	1.7
Valle de Andorra	Andorra	54.75°S, 68.22°W	198	450-600	02/2012	AND12-PB01W1	0.77
Estancia Harberton	Harberton	54.87°S, 67.22°W	26	600	02/2012	HAR12-PB01W1	0.92

625



627
628 **Figure S1. Location of Amsterdam Island (AMS), Falkland Islands (SCB, Islas Malvinas), Andorra (AND)**
629 **and Harberton (HAR).**

630

631

632 **Text S1 Core sites:**

633 **Amsterdam Island (AMS):** A 5 m-long peat sequence (AMS14-PB01A) was collected from the most
634 elevated area of the peatland at 738 m a.s.l. in December 2014 using a stainless steel Russian D-corer of
635 10 cm internal diameter and 50 cm length. The mean annual temperature at the meteorological station
636 (27 m a.s.l.) is 14°C and annual precipitation is about 1100 mm yr⁻¹ (ref¹). For details about AMS coring site
637 see ref². The vegetation at the coring site is characterized by bryophytes (brown mosses together with
638 liverworts and some *Sphagnum* species), *Blechnum penna-marina*, *Scirpus aucklandicus*, *Trisetum insularis*
639 and scattered stands of *Agrostis delislei*. Based on low resolution plant macrofossil data for the last 1000
640 years of a peat core taken close to the AMS14-PB01A core, with an independent age-depth model, the
641 macrofossil record is dominated by higher plant epidermis (c. 70%) until about 400 cal yr BP. For the last
642 400 years, bryophytes are dominant (70-80%), mainly composed of brown mosses and liverworts, with
643 little occurrence of *Sphagnum* spp. Ash content is <2wt% throughout the core and, together with major
644 element profiles, suggests the site to be ombrotrophic to at least 3.5m depth.

645
646 **The Falkland Islands (SCB, Islas Malvinas):** 'San Carlos bog' is located on the western side of East Falkland
647 Islands (SCB13-PB01C). The native vegetation is treeless and dominated by mosses, grasses and dwarf
648 shrubs^{3,4}. A 1.7 m-long peat sequence was collected from a hummock with an upper monolith section (0
649 - 50 cm) and lower Russian core section⁵. The surface vegetation of the bog is dominated by *Sphagnum*
650 *magellanicum*, *Hymenophyllum caespitosum*, *Gaultheria pumila*, *Oreobulis obtusangulus*, *Gunnera*
651 *magellanica* and *Myrteola nummularia*. *Sphagnum* is found to be more than 80% to a depth of 65 cm and
652 followed by herbaceous compacted peat to the bottom. The annual precipitation and temperature are
653 575 mm yr⁻¹ and 7°C, respectively (data sources from the Falkland Islands Government reported in ref⁴).

654 **Andorra (AND):** An ombrotrophic peat monolith (0.72 m length, AND12-PB01W1) was collected at
655 Andorra bog using a stainless steel Wardenaar corer⁶. The AND peat profile is dominated >96% by
656 *Sphagnum magellanicum*. The annual precipitation and temperature are 450-600 mm yr⁻¹ and 6°C,
657 respectively⁷.

658 **Harberton (HAR):** An ombrotrophic peat monolith (0.73 m length, HAR12-PB01W1) was sampled at
659 Harberton Bog by a stainless steel Wardenaar corer⁶. The bog surface is dominated >80% by *Sphagnum*
660 *magellanicum* with a sparse cover of *Marsippospermum grandiflorum* and *Empetrum rubrum*⁸. The annual
661 precipitation and temperature are around 600 mm yr⁻¹ and 6°C, respectively⁸. We are aware of limited
662 gold mining from 1883 to 1906 on Chilean Islands South of the Beagle Channel, but this is hundreds of
663 km's away from our sites, and late 20th century peaks in HgAR at HAR do not correspond in terms of timing.

664

665 **Table S2 Accelerator Mass Spectrometry ¹⁴C dating of plant macrofossils from all the four peat cores.**

666

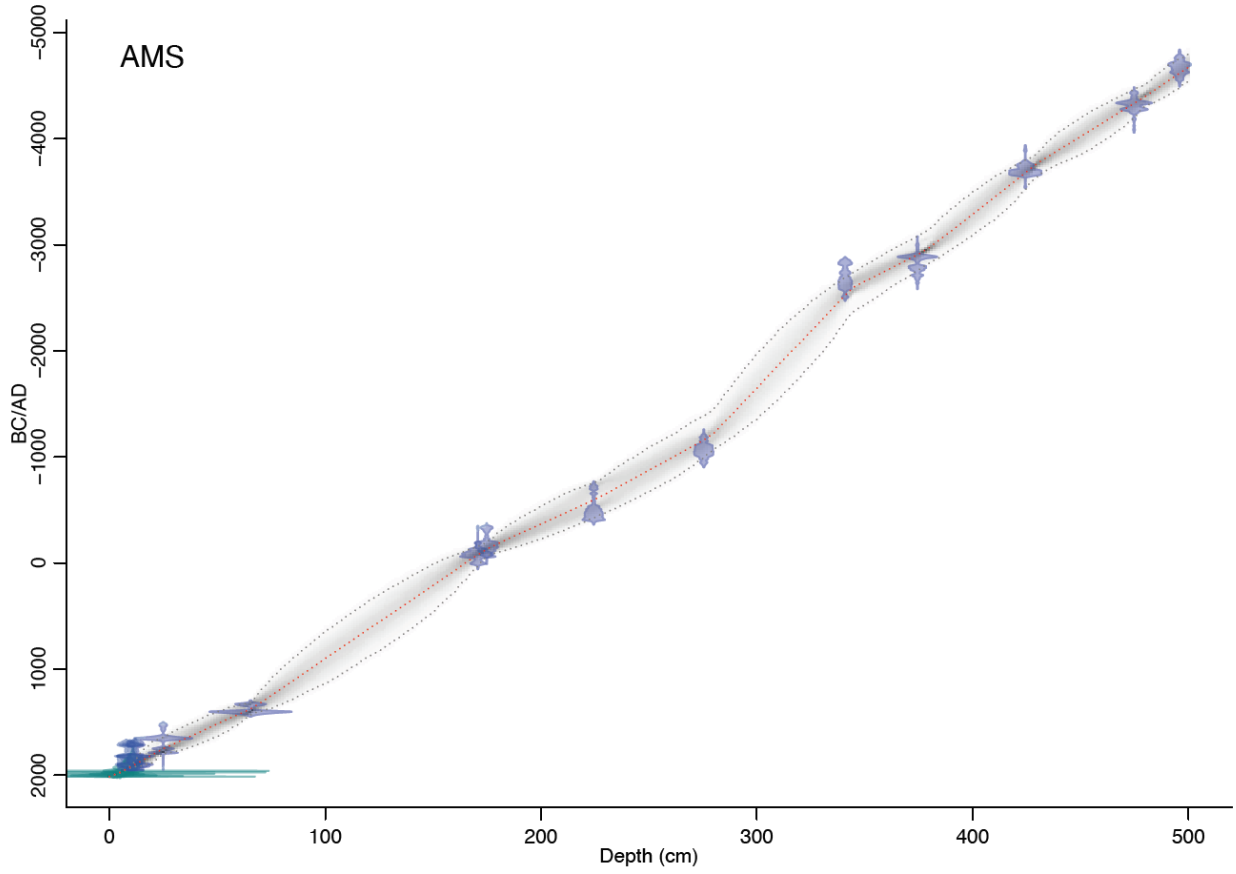
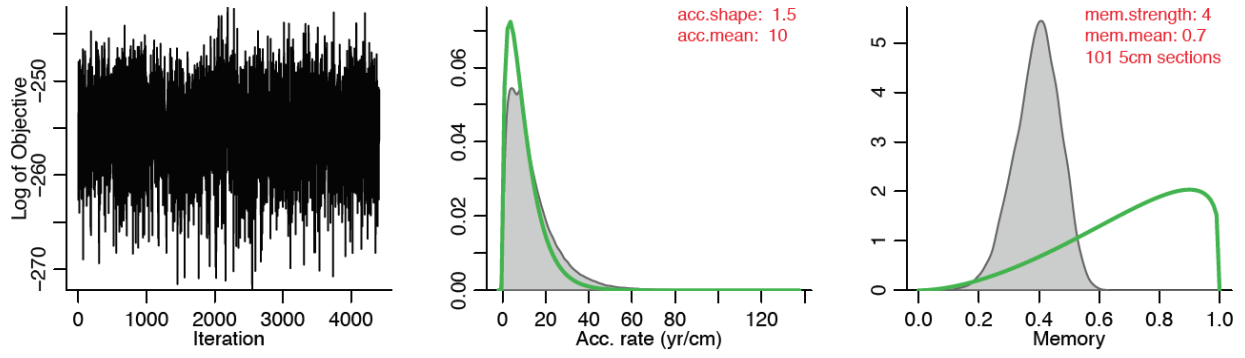
Core name	Lab ID	Mid-Point Depth (cm)	material	Conventional ¹⁴ C Age (yr BP, ± 1σ)	Calibrated age (median, AD/BC)	Modelled age AD/BC (95.4% probability range)
AMS*	SacA50049	2.0	<i>Chorisondontium/Dicranoloma</i> stems + leaves	-557 ± 21	2008 AD	1997-2001 AD
AMS*	SacA50050	3.5	Brown moss stems	-1489 ± 20	1987 AD	1985-1987 AD
AMS*	SacA50051	4.9	Brown moss + liverworts stems	-3052 ± 18	1974 AD	1973-1979 AD
AMS*	SacA50052	6.4	Brown moss + liverworts stems	-1248 ± 20	1960 AD	1956-1962 AD
AMS*	SacA50053	7.8	Brown moss stems	135 ± 30	1942 AD	1938-1950 AD
AMS*	SacA50054	9.4	Brown moss stems	115 ± 30	1928 AD	1917-1937 AD
AMS*	SacA50055	10.8	Brown moss stems + leaves	80 ± 30	1912 AD	1895-1923 AD
AMS*	SacA50056	12.0	Brown moss stems + <i>Chorisondontium/Dicranoloma</i> leaves	160 ± 30	1893 AD	1854-1917 AD
AMS*	SacA50057	13.2	brown moss stems	70 ± 30	1885 AD	1823-1915 AD
AMS*	GdA-4136	24.9	brown moss stems	275 ± 25	1752 AD	1640-1800 AD
AMS*	GdA-4558	65.4	Residue (<i>Sphagnum</i> dominated)	595 ± 25	1389 AD	1310-1440 AD
AMS*	GdA-4560	170.7	Brown moss stems	2100 ± 25	78 BC	155 BC-30 AD
AMS*	GdA-4137	174.8	brown moss stems	2170 ± 30	126 BC	195-55 BC
AMS*	GdA-4138	224.4	brown moss stems	2430 ± 30	580 BC	750-415 BC
AMS*	GdA-4139	275.4	brown moss stems	2925 ± 30	1142 BC	1380-980 BC
AMS*	GdA-4561	340.9	brown moss stems	4145 ± 35	2535 BC	2965-2275 BC
AMS*	GdA-4140	374.4	<i>Sphagnum</i>	4285 ± 30	2900 BC	3075-2750 BC
AMS*	GdA-4141	424.4	<i>Sphagnum</i> + brown moss	4960 ± 30	3680 BC	3795-3550 BC
AMS*	GdA-4142	474.8	<i>Sphagnum</i> stems	5515 ± 35	4330 BC	4460-4190 BC
AMS*	GdA-4143	495.9	<i>Sphagnum</i> stems	5860 ± 35	4615 BC	4750-4470 BC
SCB	SUERC-51676	76.5	<i>Sphagnum</i>	153 ± 37	1694 AD	1597-1737 AD
SCB	GdA-3755	99.9	Undefined peat macrofossils	814 ± 41	1256 AD	1147-1345 AD
SCB	GdA-4744	109.8	Charcoal + Monocyledons undifferentiated (leaf bases)	1553 ± 25	1009 AD	876-1152 AD
SCB	GdA-4745	123.7	Monocyledons undifferentiated (leaf bases)	1261 ± 21	804 AD	688-896 AD
SCB	GdA-4746	146.3	Monocyledons undifferentiated (leaf bases)	1661 ± 25	428 AD	277-532 AD
SCB	GdA-4742	154.3	Charcoal + Monocyledons undifferentiated (leaf bases)	2882 ± 22	252 AD	19 BC-396 AD
SCB	GdA-3756	164.3	Undefined peat macrofossils	11582 ± 50	36 AD	376 BC-254 AD
AND	SacA50058	0.6	<i>Sphagnum</i>	-594 ± 19	2004 AD	2007-2014 AD
AND	SacA50059	13.1	<i>Sphagnum</i>	-1749 ± 19	1983 AD	1985-2000 AD
AND	SacA50060	34.3	<i>Sphagnum</i>	-2839 ± 17	1974 AD	1969-1976 AD
AND	SacA50061	41.0	<i>Sphagnum</i>	-2695 ± 18	1964 AD	1961-1967 AD
AND	SacA50062	47.6	<i>Sphagnum</i>	-67 ± 21	1954 AD	1947-1958 AD
AND	SacA50063	54.6	<i>Sphagnum</i>	120 ± 30	1926 AD	1902-1942 AD
AND	SacA50064	61.9	<i>Sphagnum</i>	140 ± 30	1893 AD	1856-1919 AD
AND	SacA50065	68.8	<i>Sphagnum</i>	160 ± 30	1863 AD	1814-1893 AD
AND	GdA-3032	73.2	<i>Sphagnum</i>	193 ± 23	1843 AD	1787-1876 AD
AND	SacA50066	76.1	<i>Sphagnum</i>	150 ± 30	1831 AD	1769-1865 AD
HAR	SacA42507	0.3	<i>Sphagnum</i>	-424 ± 21	2010 AD	2010-2019 AD
HAR	SacA42508	4.7	<i>Sphagnum</i>	-606 ± 22	2004 AD	2002-2012 AD
HAR	SacA42509	6.9	<i>Sphagnum</i>	-677 ± 21	2002 AD	1999-2008 AD
HAR	SacA42510	9.1	<i>Sphagnum</i>	-788 ± 21	1999 AD	1996-2005 AD

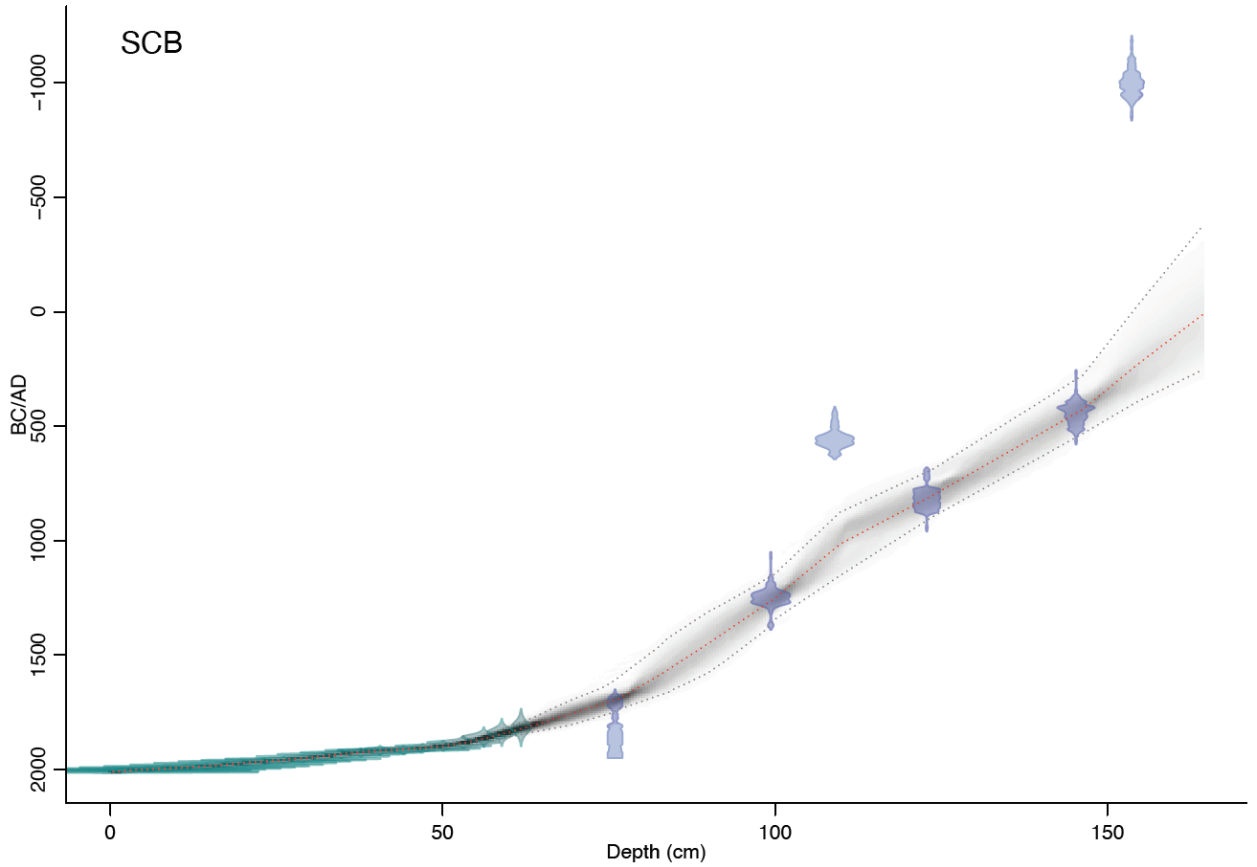
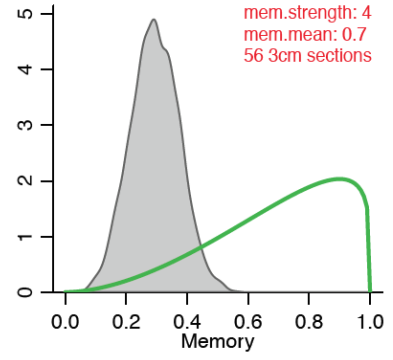
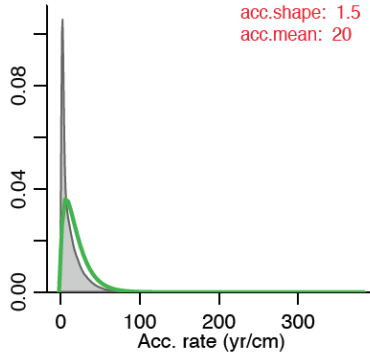
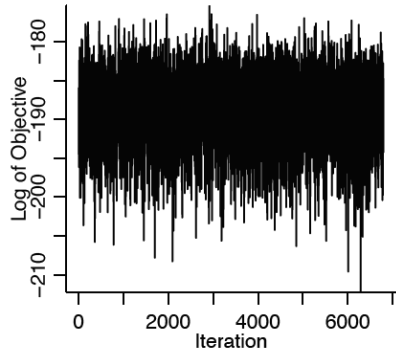
Non-peer reviewed EarthArXiv preprint

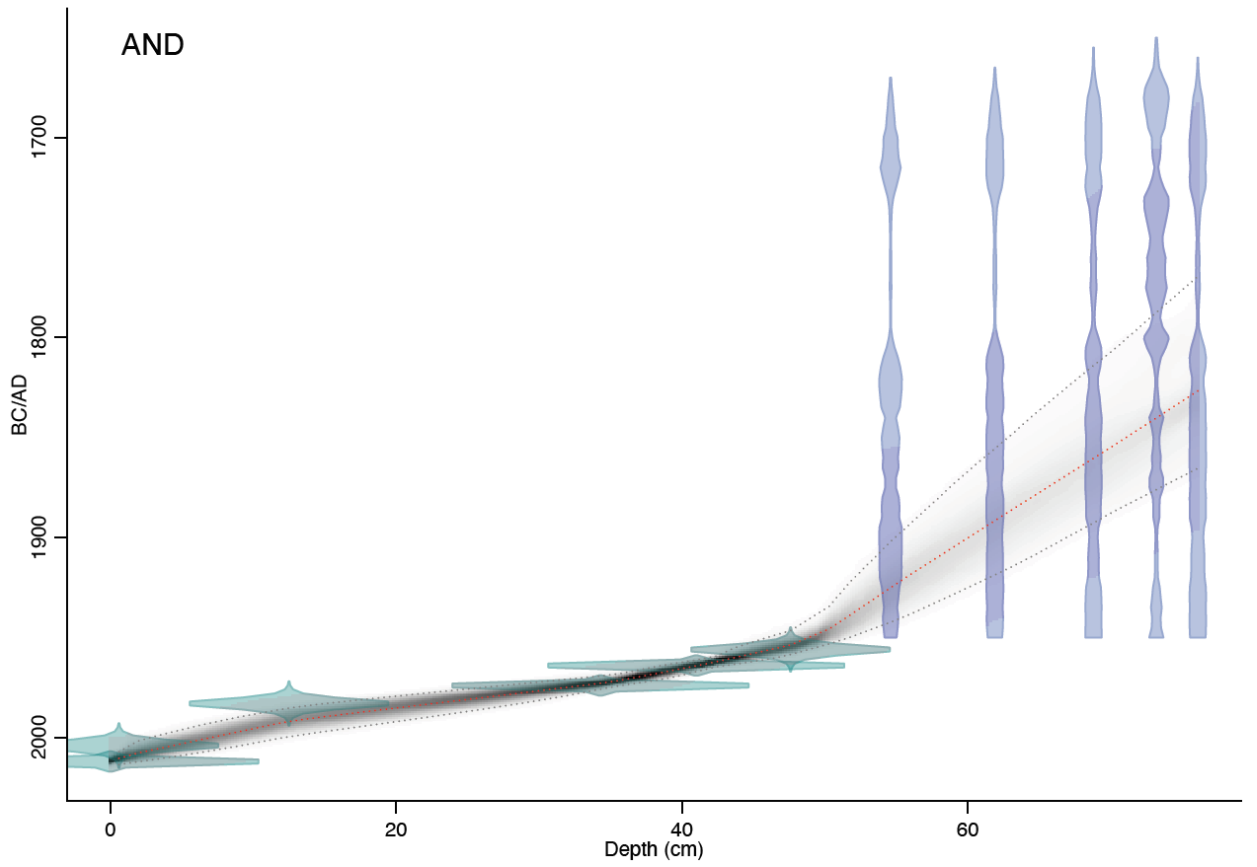
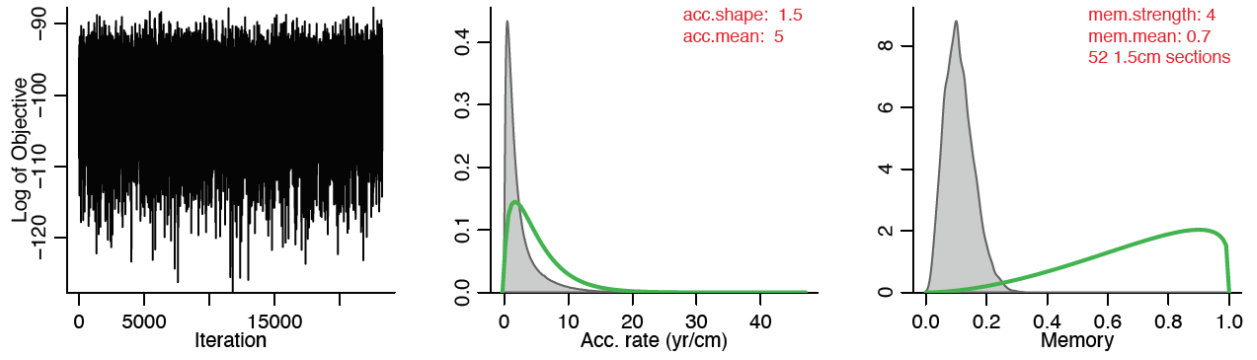
HAR	SacA42511	11.3	<i>Sphagnum</i>	-838 ± 22	1998 AD	1994-2002 AD
HAR	SacA42512	13.6	<i>Sphagnum</i>	-914 ± 21	1996 AD	1991-1999 AD
HAR	SacA44490	15.8	<i>Sphagnum</i>	-1092 ± 22	1992 AD	1988-1996 AD
HAR	SacA44491	19.2	<i>Sphagnum</i>	-1333 ± 21	1988 AD	1984-1992 AD
HAR	SacA44492	21.3	<i>Sphagnum</i>	-1513 ± 20	1985 AD	1981-1989 AD
HAR	SacA44493	26.6	<i>Sphagnum</i>	-2186 ± 21	1979 AD	1974-1982 AD
HAR	SacA44494	31.7	<i>Sphagnum</i>	-2715 ± 20	1975 AD	1964-1976 AD
HAR	SacA44495	37.0	<i>Sphagnum</i>	-2462 ± 27	1964 AD	1930-1964 AD
HAR	SacA44496	43.5	<i>Sphagnum</i>	214 ± 23	1815 AD	1736-1885 AD
HAR	SacA44497	56.2	<i>Sphagnum</i>	407 ± 25	1608 AD	1518-1631 AD
HAR	SacA44498	90.7	<i>Sphagnum</i>	984 ± 24	1148 AD	1063-1216 AD

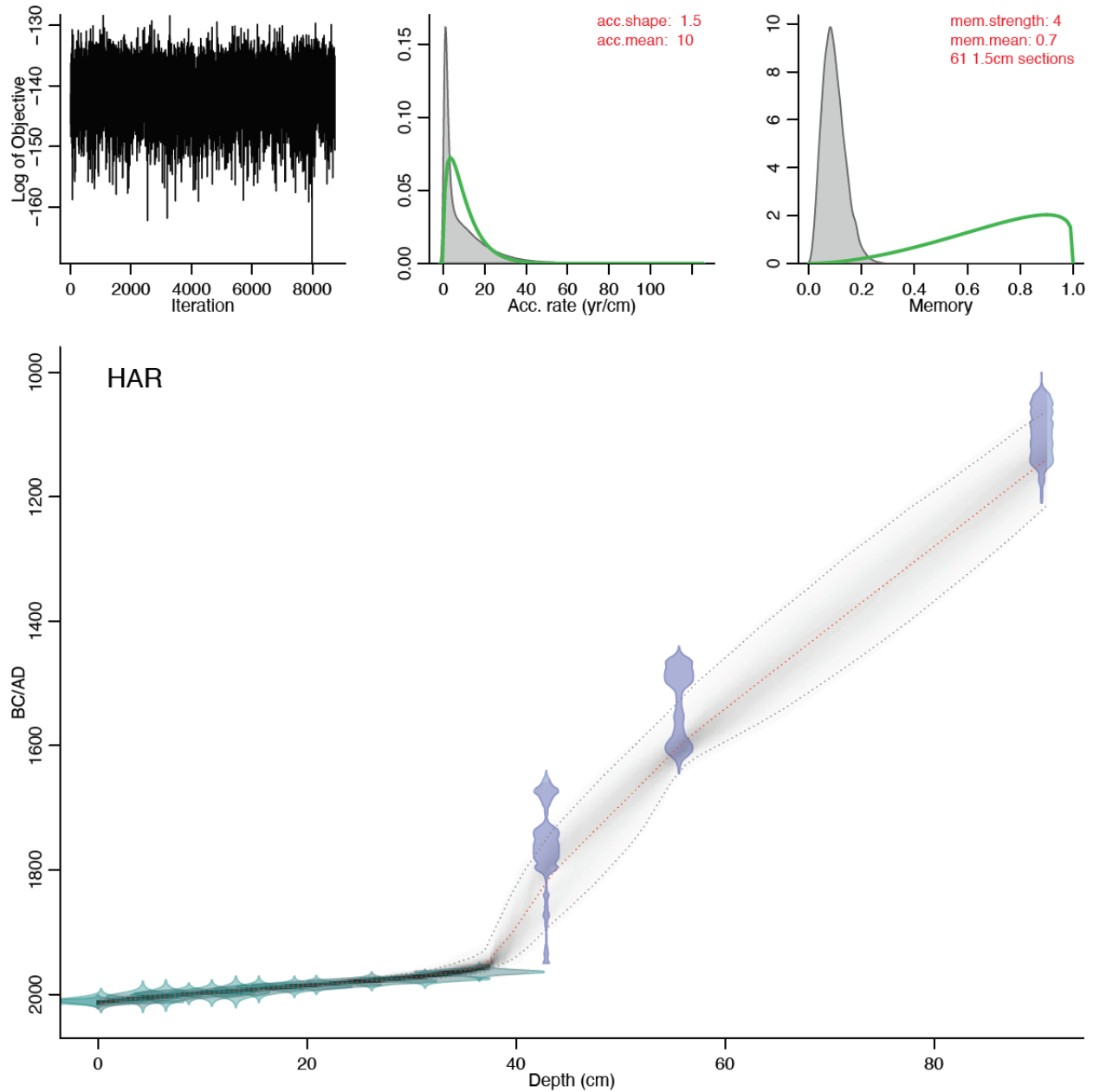
667

*Data are from ref ²⁸.









671
672

673 **Figure S2. Age models of peat cores from AMS, SCB, AND and HAR using Bacon.** Calibrated ^{14}C dates show
 674 in transparent blue and ^{210}Pb dates show in transparent green. Red curve indicates single best-fit model
 675 based on the weighted mean age for each depth. Darker greys represent more likely calendar ages with
 676 95% confidence intervals shown by grey stippled lines. Diagnostic plots in upper left panels confirm
 677 appropriate performance of the models. Settings for accumulation rate and memory are shown in middle
 678 and right upper panels (green line—prior, grey shade—posterior distribution), along with thickness and
 679 number of sections used for modelling. Prior settings for accumulation rates described by gamma
 680 distribution with shape 1.5 and acc.mean 10 or 20 yr/cm, for memory the default beta distribution with
 681 parameters mem.strength=4 and mem.mean=0.7 was used.

682

683 **Table S3 Summary of Hg measurements in standard reference materials.**

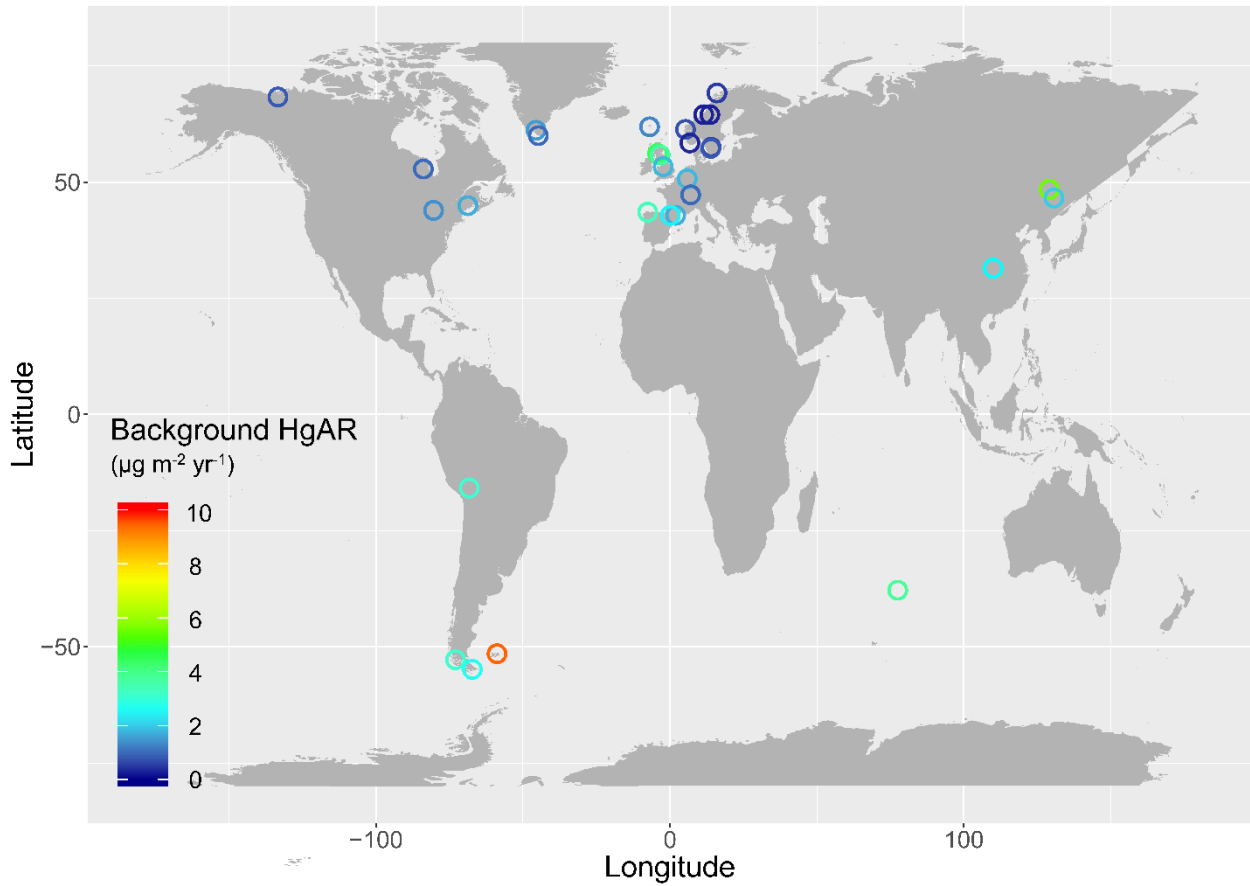
684

SRM	materials	Measured value (mean \pm 1 σ , ng g ⁻¹)	Certified value (mean \pm 2 σ , ng g ⁻¹)
IPE 176	Reed/ <i>Phragmites communis</i>	35.1 \pm 6.3 (n=143)	37.9 \pm 2.9
NIST 1632d	Coal	91.3 \pm 7.0 (n=9)	92.8 \pm 3.3
BCR 482	Lichen	481.3 \pm 8.7 (n=5)	480 \pm 20

685

686

687



688

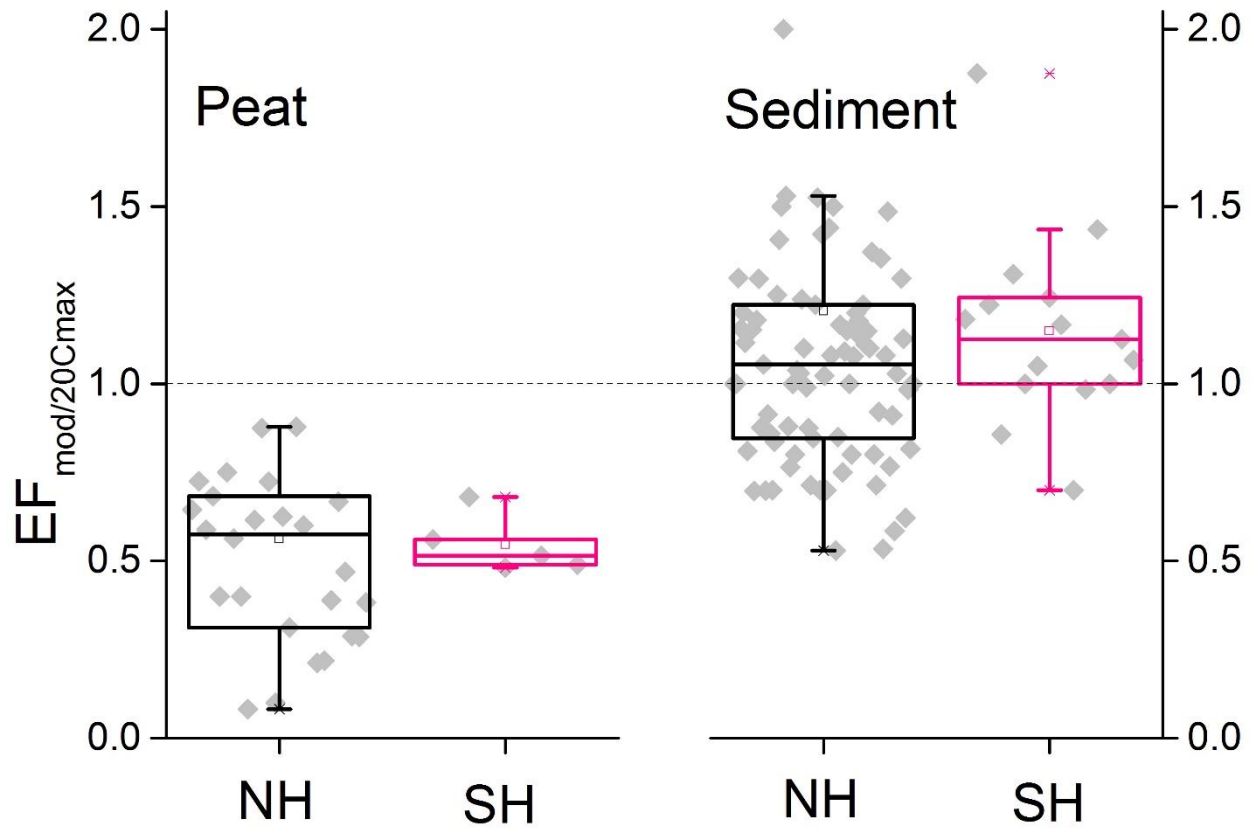
689 **Figure S3. Natural background Hg accumulation rates ($\mu\text{g m}^{-2} \text{yr}^{-1}$) derived from natural peat archives.**

690 **Details see Extended Data 2.**

691

692

693



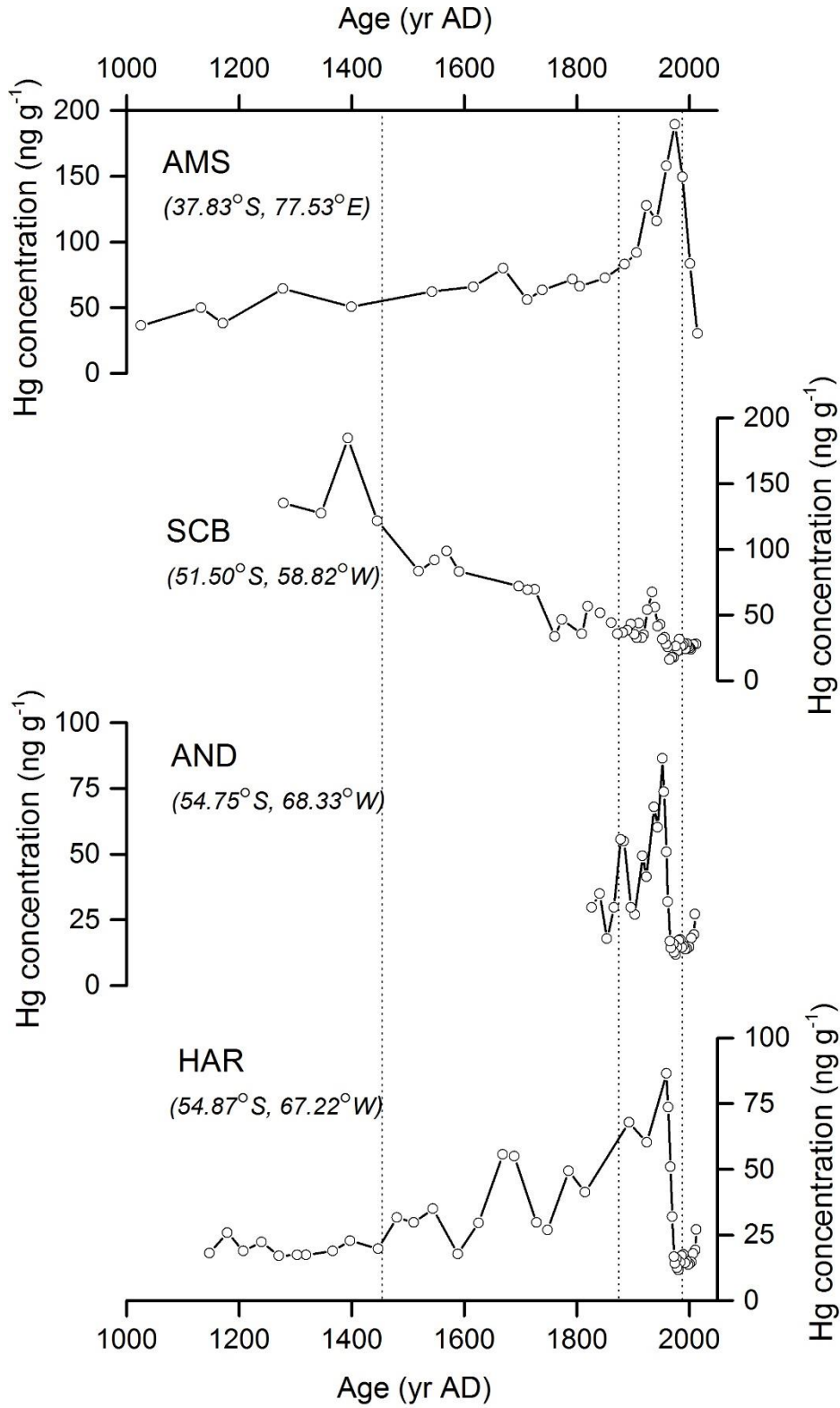
694

695

696

697 **Figure S4. Profiles of HgAR enrichment factor of modern (post-1990) to extended 20th century maximum**
698 **($EF_{\text{mod}/20\text{Cmax}}$) from Northern Hemisphere (NH) and Southern Hemisphere (SH) peat and sediment records.**
699 **Dashed line indicates $EF=1$.**

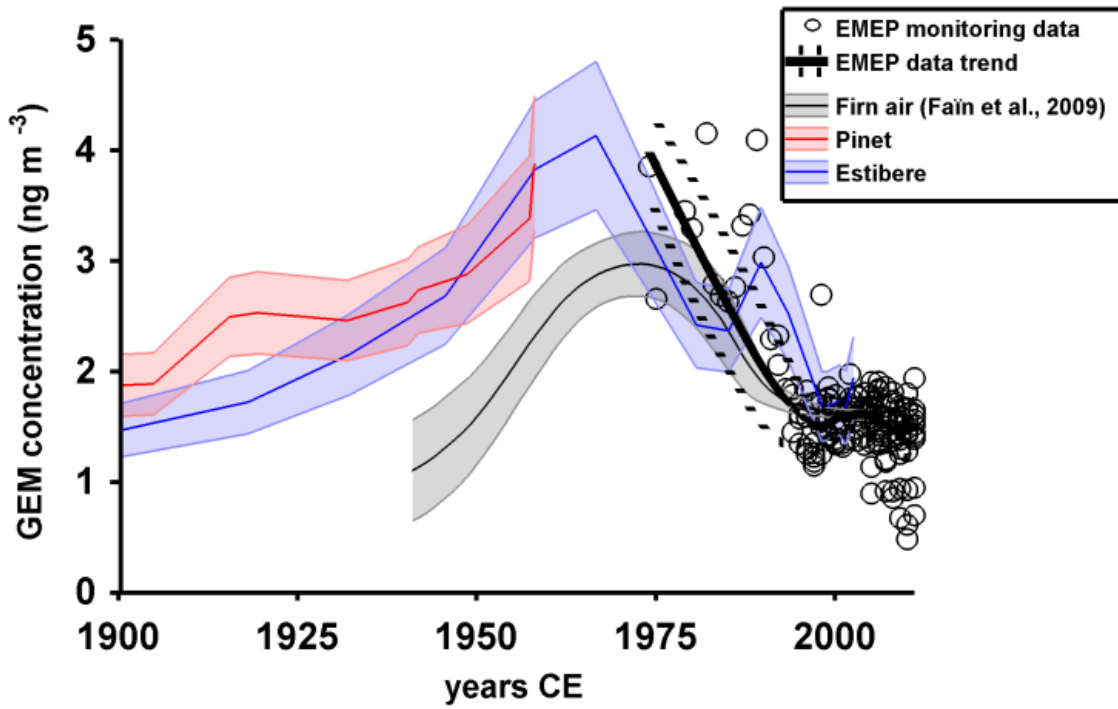
700



701

702 **Figure S5. Profiles of Hg concentration (ng g⁻¹) in the peat cores from AMS, SCB, AND and HAR.**

703



704

705 **Figure S6. Historical atmospheric Hg monitoring observations and reconstructed Hg levels.** Figure
706 reproduced from Enrico et al. 2017, ES&T with permission⁹. Atmospheric gaseous elemental Hg⁰ (GEM)
707 monitoring data (circles) are from EMEP¹⁰.

708

709 **Supporting Information references**

- 710 1. Lebouvier, M. and Frenot, Y.. Conservation and management in the French sub-Antarctic islands and
711 surrounding seas. In *Papers and proceedings of the royal society of Tasmania*. 207, Vol. 141, No. 1, pp. 23-28.
- 712 2. Li, C.; Le Roux, G.; Sonke, J.; van Beek, P.; Souhaut, M.; Van der Putten, N.; De Vleeschouwer, F. Recent
713 ²¹⁰Pb, ¹³⁷Cs and ²⁴¹Am accumulation in an ombrotrophic peatland from Amsterdam Island (Southern Indian
714 Ocean). *Journal of environmental radioactivity*. 2017, 175, pp.164-169.
- 715 3. Moore, D.M., 1968. The vascular flora of the Falkland Islands. *The vascular flora of the Falkland Islands.*, (60).
- 716 4. Bokhorst, S.; Convey, P.; Huiskes, A.; Aerts, R. Dwarf shrub and grass vegetation resistant to long-term
717 experimental warming while microarthropod abundance declines on the Falkland Islands. *Austral Ecology*. 2017,
718 42(8), pp.984-994.
- 719 5. Belokopytov, I.E. and Beresnevich, V.V. Giktorf's peat borers. *Torfyanaya Promyshlennost*. 1955, 8(9), p.10.
- 720 6. Wardenaar, E.C.P. A new hand tool for cutting soil monoliths. *Canadian journal of Soil science*. 1987, 67(2),
721 pp.405-407.
- 722 7. Mauquoy, D.; Blaauw, M.; Van Geel, B.; Borronei, A.; Quattrocchio, M.; Chambers, F.M.; Possnert, G. Late
723 Holocene climatic changes in Tierra del Fuego based on multiproxy analyses of peat deposits. *Quaternary Research*.
724 2004, 61(2), pp.148-158.
- 725 8. Vanneste, H., De Vleeschouwer, F.; Martínez-Cortizas, A.; Von Scheffer, C.; Piotrowska, N.; Coronato, A.; Le
726 Roux, G. Late-glacial elevated dust deposition linked to westerly wind shifts in southern South America. *Scientific*
727 *reports*. 2015, 5, p.11670.
- 728 9. Enrico M., et al., Holocene Atmospheric Mercury Levels Reconstructed from Peat Bog Mercury Stable
729 Isotopes. *Environ. Sci. Technol*. 2017, 51, 5899–5906.
- 730 10. European Monitoring and Evaluation Programme (2016). <https://www.emep.int/>

731

732

733

734

735

736

737